

Understanding the effect of hyperparameter optimization on machine learning models for structure design problems

Xianping Du¹⁺, Hongyi Xu², Feng Zhu^{1,3*}

1 Department of Mechanical Engineering, Embry-Riddle Aeronautical University, Daytona Beach, FL 32114, USA

2 Department of Mechanical Engineering, University of Connecticut, Storrs, CT 06269, USA

3 Hopkins Extreme Materials Institute and Department of Mechanical Engineering, Johns Hopkins University, Baltimore, MD, 21218, USA

Abstract:

To relieve the computational cost of design evaluations using expensive finite element (FE) simulations, surrogate models have been widely applied in computer-aided engineering design. Machine learning algorithms (MLAs) have been implemented as surrogate models due to their capability of learning the complex interrelations between the design variables and the response from big datasets. Typically, an MLA regression model contains model parameters and hyperparameters. The model parameters are obtained by fitting the training data. Hyperparameters, which govern the model structures and the training processes, are assigned by users before training. There is a lack of systematic studies on the effect of hyperparameters on the accuracy and robustness of the surrogate model. In this work, we proposed to establish a hyperparameter optimization framework to deepen our understanding of the effect. Four frequently used MLAs, namely Gaussian Process Regression (GPR), Support Vector Machine (SVM), Random Forest Regression (RFR), and Artificial Neural Network (ANN), are tested on four benchmark examples of structure design optimization. For each MLA model, the model accuracy and robustness before and after the hyperparameters optimization (HOpt) are compared. The results show that HOpt can generally improve the performance of the MLA models in general. HOpt leads to few improvements in the MLAs accuracy and robustness for complex problems, which are featured by high-dimensional mixed-variable design space. The HOpt is recommended for the design problems with intermediate complexity. We also investigated the additional computational costs incurred by HOpt. The training cost is closely related to the MLA architecture. After HOpt, the training cost of ANN and RFR is increased more than that of the GPR and SVM. To sum up, this study benefits the selection of HOpt method for the different types of design problems based on their complexity (i.e. design domain continuity and the number of design variables, etc.).

Keywords: Structure design; Surrogate models; Machine learning; Hyperparameters optimization; Gaussian process regression; Support vector machine; Random forest regression; Artificial neural network

⁺ Current affiliation: Department of Mechanical and Aerospace Engineering, Rutgers University, Piscataway, NJ 08854, USA

^{*} Corresponding author: Hopkins Extreme Materials Institute, Johns Hopkins University, 3400 N Charles St, Baltimore, MD 21218, USA

E-mail: fengzhume@gmail.com (Dr. Feng Zhu); [Xianping Du \(DUX1@mv.erau.edu\)](mailto:DUX1@mv.erau.edu); [Hongyi Xu \(hongyi.3.xu@uconn.edu\)](mailto:hongyi.3.xu@uconn.edu)

1. Introduction

In the development of complex structures, such as a vehicle or aircraft, a large number of full-scale numerical simulations are often needed. As the supplement and partial substitute of these expensive simulations, surrogate models have been widely used in engineering design and optimization to reduce the computational cost [1-3]. A surrogate model is established from the design or simulation datasets through regression, to approximate the real model. It provides an efficient way of predicting the responses of new design alternatives without running additional simulations [4]. Surrogate-based methods have been applied successfully in engineering practices, for example, vehicle crashworthiness design [5], crane bridge optimization [6], transportation facility design [7] and so on. To be adapted to various engineering problems, which are characterized by a different number of design variables, degree of nonlinearities, and loading rates and so on, several surrogate models have been proposed, such as a polynomial response surface model, radial basis function and Kriging model [5]. However, it is difficult, if not possible, to use one surrogate modeling method to provide accurate predictions for all types of problems [8]. Therefore, much effort was made on the selection of a suitable algorithm for a specific engineering problem [8-10], and the ensemble and aggregation of multiple surrogate models [11-15] for a higher modeling accuracy.

To comply with the requirement of surrogate modeling with higher accuracy, MLAs have been applied to implement surrogate models for a wide range of problems due to their powerful learning ability and high flexibility [8, 10, 16-20]. The traditional surrogate methods contain only model parameters that can be fitted by data. For example, the constants of the linear regression can be determined by the least square error method; polynomial response surface parameters can be determined by gradient-based methods. Unlike the traditional surrogate modeling approaches, a typical MLA contains not only model parameters but also hyperparameters [21-23], which have to be assigned before model training to control the training process and model structures. They have a great impact on model flexibility, accuracy, and robustness [22-25].

Up to date, no systematic studies have been conducted regarding the effect of hyperparameters on the MLA-based surrogate modeling in engineering design. Most of the existing studies [26], which applying MLAs as surrogate models, either directly use the default values provided by the MLA package [27], or determine their values based on experience [28] or trial-and-error [29]. Although these surrogate models

were trained with good accuracy under pre-determined loss function(s), the potential of the MLAs has not been fully exploited and the way that hyperparameters affect the surrogate modeling performance has not been clarified. To analyze the influence of hyperparameters on the prediction performance, several studies have been performed by parametric analysis in various areas, including the biomechanical analysis [30], material design [31] and mineral exploration [32]. In these studies, however, only a small portion of hyperparameters were tuned from a specific dataset, and the final values of hyperparameters were determined subjectively. Also, the effect of MLA hyperparameters has not been investigated in the area of structural design. Lacking this knowledge, it would be very difficult to fully understand and improve the surrogate modeling of MLAs in the structural design practice. Furthermore, the potential of MLAs cannot be fully exploited solely by traditional parametric studies [33]. The HOpt in structural design is therefore needed. HOpt, which adapts the optimization methods in hyperparameters tuning by taking the hyperparameters as design variables, has been considered as an effective technique to search optimal values of selected hyperparameters. With the help of HOpt, the great improvement of MLAs prediction accuracy has been confirmed on many public datasets [23-25, 34]. However, no studies have been reported on HOpt in structure engineering.

In this work, by developing a multi-objective HOpt framework, the effort is made to analyze the surrogate modeling performances of four frequently used MLAs, namely, Gaussian Process Regression (GPR), Support Vector Machine (SVM), Random Forest Regression (RFR), and Artificial Neural Network (ANN). These MLAs are selected as they are widely applied in structural engineering problems, as summarized in Table 1 [13, 28, 29, 32, 35-57]. After a discussion of their accuracy, training cost, and model robustness before and after the HOpt, the hyperparameters tuning of two superior MLAs are also discussed.

The remaining parts of this work are organized as follows. Section 2 introduces the basic algorithms of the four MLAs under the context of surrogate modeling. The HOpt framework is described in detail in Section 3 and then it is used to formulate the HOpt for the four MLAs in Section 4. Four engineering benchmark structures are selected and introduced in Section 5, where the simulation datasets are generated. The optimization processes are completed, and the results are presented and analyzed in Section 6 to investigate the hyperparameters effect on modeling accuracy and training cost. A further discussion in

Section 7 reveals the effect of HOpt on the surrogate model robustness. Besides, parametric studies on the hyperparameters of two superior MLAs, GPR and ANN, are conducted and the results are summarized and documented in the supplement file.

Table 1 Literature on the machine learning algorithms applied as surrogate models in structural engineering

Literature	Algorithm	Application	Hyperparameters assignment
<u>Mukherjee, A. et al (1995) [35]</u>	ANN	RC beam design	Experience and trail-and-error
<u>Kapania, R. K. et al (1998) [36]</u>	ANN	An aerospace continuum beam design	Trail-and-error
<u>Nagendra, S. et al (2004) [37]</u>	ANN	A turbine disk performance prediction	Trail-and-error
<u>Lee, J. et al (2007) [38]</u>	ANN	A suspension design	Experience and optimization
<u>Tang, Y. C. et al (2009) [39]</u>	SVM	The robust design of sheet metal forming process	Experience
<u>Guo, Z. et al (2009) [40]</u>	SVM	Reliability analysis for huge space station	Not mentioned
<u>Pan, F. et al (2010) [28]</u>	SVM	B-pillar weight minimization using tailor-welded blank (TWB) structure u	Experience
<u>Wang, H. et al (2010) [41]</u>	LS-SVM ^a	The response prediction of a cylinder and whole vehicle crash	Not mentioned
<u>Huang, Z. et al (2011) [42]</u>	GPR ^b	Optimal design of aero-engine turbine disc	Experience
<u>Zhu, P. et al (2012) [29]</u>	SVM	Design of vehicle structures for lightweight and crashworthiness	Trail-and-error
<u>Zhang, Y. et al (2012) [43]</u>	GPR	Crashworthiness optimization of a foam-filled bitubal square column	Experience
<u>Haleem, K. et al (2013) [44]</u>	RFR	To predict the severity of traffic accident	Experience
<u>Song, X. et al (2013) [45]</u>	RSM ^c , GPR, SVM, and RBF ^d	A foam-filled tapered thin-walled structure response prediction	Experience
<u>Yin, H. et al (2014) [46]</u>	RSM, RBF, GPR, and SVM	A foam-filled thin-walled structure	Experience
<u>Lukaszewicz, D. et al (2014) [47] and (2015) [48]</u>	RFR	Prediction of structure impact performance under manufacturing variation	Not mentioned
<u>Rodríguez-Galiano, V. et al (2014) [49] and (2015) [32]</u>	ANN, DT ^e , RFR, and SVM & RFR	Used to map the statistical distribution of mineral prospectivity based on images	Trail-and-error
<u>Fang, J. et al (2014) [50]</u>	GPR	To explore the multi-objective design of foam-filled bitubal structures under uncertainty	Trail-and-error
<u>Ferreira, W. G. et al (2015) [13]</u>	RSM, GPR, RBNN ^f , and SVM	Analytical and real-world vehicle crashworthiness analysis	Experience
<u>Fang, J. et al (2015) [51]</u>	GPR	For the multi-cell tubes optimization	Not mentioned

<u>Tang, Z. et al (2016) [52]</u>	RFR	Response prediction of train sets crash with respect to different parameters	Experience
<u>Liu, X. et al (2016) [53]</u>	GPR	Demonstrated by a thin-walled box beam and a long cylinder pressure vessel example	Not mentioned
<u>Raihan, M. et al (2018) [55]</u>	RFR	Used to find important variables explaining clustered traffic accident data	Not mentioned
<u>Duan, L. et al (2018) [56]</u>	SVM	Multi-objectives optimization of a new vehicle longitudinal beam	Experience
<u>Palar, P. S. et al (2018) [57]</u>	GPR	The airfoil models design	Optimization
<u>Gong, H. R. et al (2018) [58]</u>	RFR	Predicting the international roughness index of asphalt pavements	Trail-and-error
<u>Fournier, E. et al (2018) [59]</u>	RFR	Predicting aeronautics loads of a derivative aircraft	Optimization

Note: ^a LS-SVM: Least Square-SVM; ^b GPR is also known as the Kriging method with almost the same basic function. ^c RSM: Response Surface Method; ^d RBF: Radial Basis Function; ^e DT: Decision tree; ^f RBNN: Radial Basis Neural Network;

2. Applying MLAs as surrogate models for engineering designs

In this section, four MLAs, i.e. the GPR, SVM, RFR, and ANN, are selected and briefly introduced in the context of surrogate-based engineering design. The design variables are expressed as $\mathbf{x} \in \mathbf{R}^n$ (real value space with n dimensions), and the responses are denoted as $\mathbf{y} \in \mathbf{R}^m$.

2.1 Gaussian Process Regression (GPR)

GPR is a non-parametric regression algorithm through Gaussian processes (GP) and takes the function as a sample in GP and can be expressed as,

$$\mathbf{y} = f(\mathbf{x}) + \varepsilon, \quad (1)$$

where, $\varepsilon \sim N(0, \sigma^2)$ is a random noisy variable. The prior distribution of $f(\mathbf{x})$ is assumed to be a zero-mean Gaussian distribution (in Equation 2) to simplify the modeling process since the mean value can be fitted easily. Hence, GPR only models the residual errors by

$$f(\mathbf{x}) \sim \mathcal{GP}(0, k(\mathbf{x}, \mathbf{x}')), \quad (2)$$

where $k(\mathbf{x}, \mathbf{x}')$ denotes covariance function. The training set is $\mathbf{T} = (\mathbf{X}, \mathbf{Y})$, so any set of new or test input \mathbf{X}^* have joint multivariate Gaussian distribution with \mathbf{T} in the form

$$\begin{bmatrix} f(\mathbf{X}), f(\mathbf{X}^*) \end{bmatrix} \mid \begin{bmatrix} \mathbf{X}, \mathbf{X}^* \end{bmatrix} \sim N\left(\mathbf{0}, \begin{bmatrix} \mathbf{K}(\mathbf{X}, \mathbf{X}) & \mathbf{K}(\mathbf{X}, \mathbf{X}^*) \\ \mathbf{K}(\mathbf{X}^*, \mathbf{X}) & \mathbf{K}(\mathbf{X}^*, \mathbf{X}^*) \end{bmatrix}\right). \quad (3)$$

The predicted $f(\mathbf{X}^*)$ is also a Gaussian distribution,

$$f(X^*) \Big| \left[f(X), X, X^* \right] \sim N(\mu^*, \Sigma^*), \quad (4)$$

where,

$$\mu^* = K(X^*, X)K(X, X)^{-1}Y, \quad (5)$$

$$\Sigma^* = K(X^*, X^*) - K(X^*, X)K(X, X)^{-1}K(X, X^*), \quad (6)$$

where \mathbf{K} is kernel functions, such as the linear, polynomial, exponential, Gaussian and Laplacian kernels [32, 60, 61]. Kernels define the basic element of GPR. Thus, kernel functions and their parameters in Equation 16 are tunable.

2.2 Support Vector Machine (SVM)

Unlike GPR, SVM seeks to fit the response linearly. However, a complex structure often exhibits nonlinear responses. Therefore, SVM tries to map design variables to a new space with higher (h) dimensions (Figure 1), where a linear regression can be realized in Equation 7.

$$f(\mathbf{x}) = \boldsymbol{\omega}^T \mu(\mathbf{x}) + b, \quad (7)$$

where $\mu(\mathbf{x})$ is the mapping function: $\mathbf{x} \rightarrow \mu(\mathbf{x}) \in \mathbb{R}^h$.

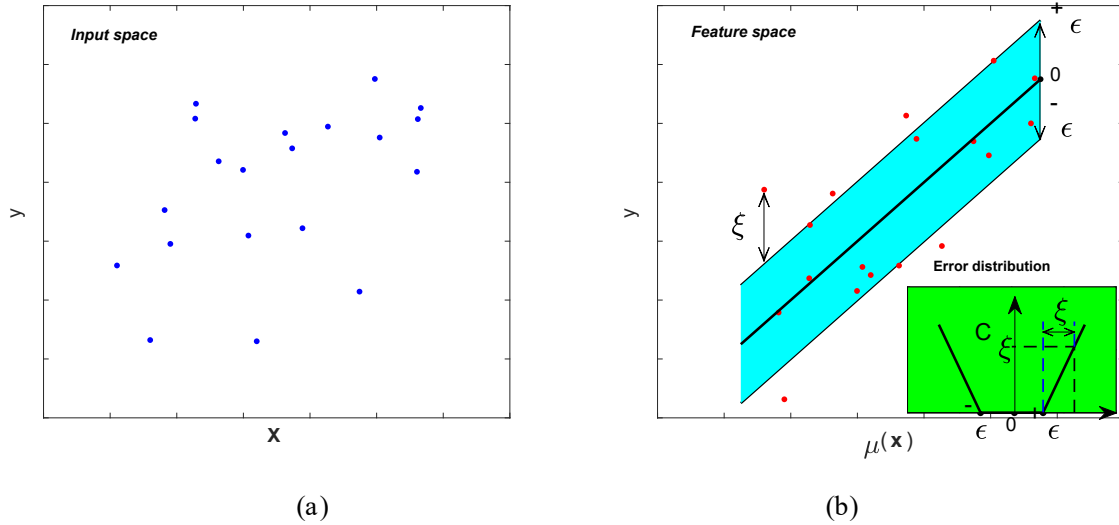


Figure 1 Process of design space mapping in the SVM: the original data in input space on the left (a) is mapped to a feature space with higher dimensions on the right (b)

The training objective compromises model complexity and accuracy by Equation 8. The complexity [62, 63] is controlled by the first term, namely, $\frac{1}{2} \boldsymbol{\omega}^T \boldsymbol{\omega}$. The second term manages the error by the

Vapnik's ε -intensive cost function to penalize the data points outside ε -bands [64] in Figure 1(b) under the constraints in Equation 9.

$$\min \quad \frac{1}{2} \boldsymbol{\omega}^T \boldsymbol{\omega} + C \sum_{i=1}^N (\xi_i + \xi_i^*) \quad (8)$$

subject to:

$$\begin{cases} y_i - (\boldsymbol{\omega}^T \boldsymbol{\mu}(\mathbf{x}_i) + b) \leq \varepsilon + \xi_i \\ (\boldsymbol{\omega}^T \boldsymbol{\mu}(\mathbf{x}_i) + b) - y_i \leq \varepsilon + \xi_i^* \\ \xi_i, \quad \xi_i^* \geq 0 \end{cases} \quad (9)$$

where C is the weight of error penalization. ξ_i and ξ_i^* are two slack variables, introduced by Cortes and Vapnik et al. [64], to take points out of the ε -bounds back to constraints. The Lagrange method is used by introducing constraints into the objective through Lagrange multiplier α and α^* [62, 64] and solving a dual problem by the quadratic programming procedure with the solution in Equation 10,

$$f(x) = \sum_{i=1}^n (\alpha_i - \alpha_i^*) \langle \boldsymbol{\mu}(\mathbf{x}_i), \boldsymbol{\mu}(\mathbf{x}) \rangle + b, \quad (10)$$

where the dot product, $K(x_i, x) = \langle \boldsymbol{\mu}(\mathbf{x}_i), \boldsymbol{\mu}(\mathbf{x}) \rangle$, defines the kernel function and the kernel functions and related parameters are tunable.

2.3 Random Forest Regression (RFR)

Random forest for regression was developed by growing a large number of tree-like data structures (termed as “trees”) [65] with numerical labels [66]. The nodes on the tree split the dataset into partitions based on a splitting criterion [65]. The RFR is also a non-parametric method to use the unweighted average of all trees' outputs as the overall output in Equation 11. Different from other methods, it can take the categorical variables directly rather than transfer them to numerical values.

$$\mathbf{y} = \mathbf{f}(\mathbf{x}) = \frac{1}{N_R} \sum_{d=1}^{N_R} \mathbf{D}_d(\mathbf{x}), \quad (11)$$

where N_R is the pre-defined number of trees; $\mathbf{D}_d(\mathbf{x})$ is the output of the d th tree.

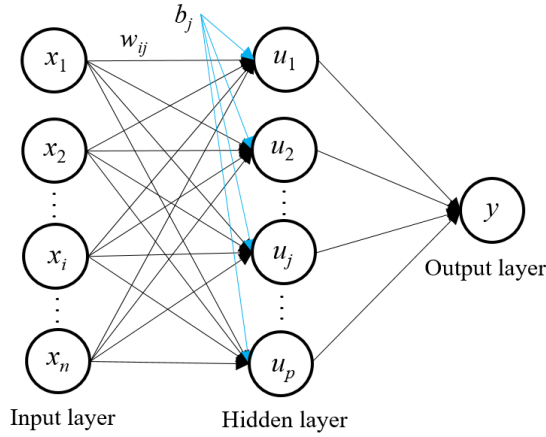
The bagging technique [66] is used in training, where a subset is sampled from the training dataset with replacement. This subset is used to train a tree and then repeat this process to generate a group of trees. This increases the diversity of trees and improve RFR robustness [32] with the generalization error reduced [66]. The structure related parameters, e.g. the number of trees, are tuned as summarized in Table 2.

2.4 Artificial Neural Network (ANN)

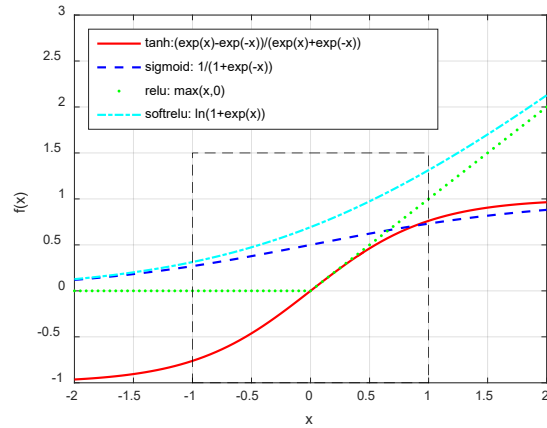
The ANN is inspired by the bio-neural system with interconnected neurons. In general, an ANN contains one input layer, multiple hidden layers, and one output layer. They are fully connected by neurons in each layer. For an ANN with a single hidden layer in Figure 2(a), the sum of weighted (w_{ij}) design variables (x_i) is taken as the input of j th hidden neuron. An activation function is defined to calculate the output of each neuron by Equation 12, where b_j is a bias. The outputs of all n_h hidden neurons are weighted as the model output in Equation 13. The weights and biases, as model parameters, are trained by data to predict new designs' responses. Several common activation functions, e.g., *tanh*, *sigmoid*, *relu*, and *softrelu* [33, 67] are shown in Figure 2(b).

$$u_j = f\left(\sum_{i=1}^n w_{ij} x_i + b_j\right), \quad (12)$$

$$y = f(x) = \sum_{j=1}^{n_h} w_{jo} u_j, \quad (13)$$



(a)



(b)

Figure 2 (a) General structure of ANN and (b) Graphic illustrations showing the example characteristics of four activation functions for ANN hidden neurons

By searching weights and biases, ANN training aims to find a local minimum of a pre-defined measure, using the gradient method. The optimizers, such as *sgd* and *adagrad*, [33, 67], control the searching process. The optimizers, activation functions, number of hidden neurons are tunable.

3. The framework of multi-objective hyperparameters optimization

The framework of a multi-objective HOpt was established based on the characteristics of MLAs and design problems [24, 25]. The sequential model-based optimization (SMBO) [21, 68] was used as the basic method as it can reach the optimum efficiently. For a specific MLA, the HOpt problem was formulated first to determine the objective(s) (i.e. searching criteria), tuned hyperparameters and ranges. The design of experiments (DoE), i.e. multiple combinations of hyperparameters, are generated and evaluated by training the corresponding MLA. The model accuracy quantified by the predefined measures of accuracy is considered as the response of each DoE. Based on this hyperparameters dataset, a surrogate model is trained to represent the relation between the hyperparameters and accuracy measures. In this study, RFR is used as the surrogate model to fit measure values with respect to hyperparameters since it could deal with the categorical features directly, for example, the selection of GPR and SVM kernels and ANN activation functions. The other surrogate methods is less flexible and deal with categorical data by converting to numerical values.

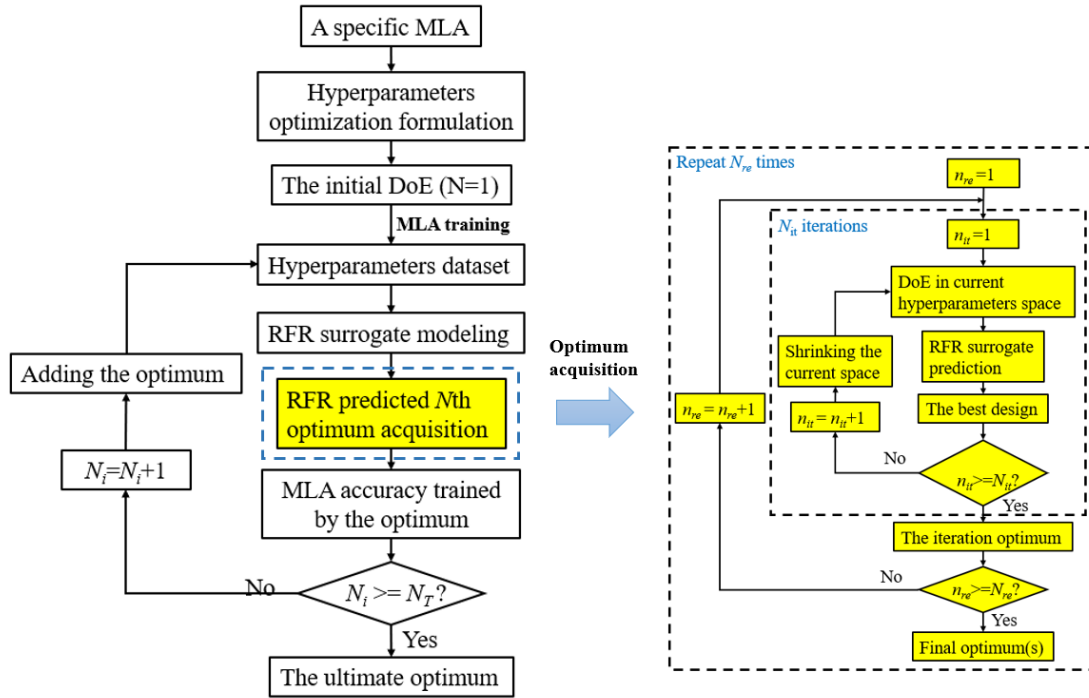


Figure 3 The framework for the multiobjective HOpt based on the sequential model-based method and the detailed workflow of the optimum acquisition

Using the constructed RFR surrogate model, the optimal hyperparameters are predicted and evaluated by training their MLA. The tuning process is terminated when the termination criterion, e.g., the maximum number of iterations (N_T), is reached. Otherwise, this optimal design will be added to the hyperparameters dataset and then update the RFR surrogate model for the next HOpt iteration. Finally, a Pareto front can be generated.

In Figure 3, the core part is the optimum acquisition with details introduced as follows. Based on the accuracy measure responses, a number of effective search criteria can be generated as objectives to achieve the trade-off between the exploration and exploitation, for example, the individual or combination of expected improvement (EI), GP upper confidence bound, the maximum possibility of improvement, minimum conditional entropy and the lower confidence bound (LCB) [24, 25, 69]. In this study, the LCB is used, and it is defined as,

$$LCB(\mathbf{x}_{hp}, \varphi) = \hat{\mu}(\mathbf{x}_{hp}) - \varphi \hat{s}(\mathbf{x}_{hp}), \quad (14)$$

where \mathbf{x}_{hp} is the vector of hyperparameters and the $\hat{\mu}(\mathbf{x}_{hp})$ and $\hat{s}(\mathbf{x}_{hp})$ are the posterior mean and standard deviation of accuracy measures, respectively, from the five cross-validations. φ is a constant to count the weight of $\hat{s}(\mathbf{x}_{hp})$, where $\varphi = 1$ is used for MLA with all numerical hyperparameters and φ equals 2 if at least one hyperparameter is categorical. This count the possible larger variation caused by categorical hyperparameter(s). $\hat{\mu}(\mathbf{x}_{hp})$ will be estimated by the RFR surrogate output directly, but $\hat{s}(\mathbf{x}_{hp})$ should be approximated by multi-responses generated by bagging technique as introduced in Section 2.3. This criterion demonstrates the lower bound of the accuracy measures reflects the error induced by RFR prediction ($\hat{s}(\mathbf{x}_{hp})$).

Using LCBs as objectives, the multi-objective HOpt will be implemented by using a design space shrinking procedure recursively. Within a single iteration, a group of designs (hyperparameters combinations) will be sampled randomly in the design space of this iteration and their response is predicted by the RFR surrogate model. The best alternative will be selected and a smaller subspace will be generated around this point. The construction of the new subspace needs to consider both exploration and exploitation. A small subspace improves convergence speed but may lose the optimum. Similarly, a larger subspace may seize the optimum but causes a low convergence speed. In this study, the $(i+1)$ th subspace is

defined as $\mathbf{x}_{hp_i} \cap \mathbf{X}_{hp_i}^* \pm \mathbf{r}_p \cdot |\mathbf{x}_{hp_i}|$, where \mathbf{x}_{hp_i} and $|\mathbf{x}_{hp_i}|$ represent the hyperparameters space of the i th iteration and its sizes and $\mathbf{X}_{hp_i}^*$ is the optimum of i th iteration. \cap and \mathbf{r}_p are the intersection operation of two subspaces and a proportion to define the expanded space size centered on the best design of the current iteration. In this smaller subspace, a new round of sampling and evaluation process will be implemented until the termination criterion is reached. The total number of the space shrinking iteration is limited to n_{it} . After the iterations are terminated, an optimum design can be obtained.

To fully explore the design space and improve robustness, this optimization process will be repeated n_{re} times. Then, a group of designs is generated by taking the Pareto front from each of the n_{re} optimization processes, where each process is implemented with n_{it} iterations for space shrinking as described above. The overall Pareto front will be obtained from this group of designs and used to determine the hyperparameter values of corresponding MLA models.

4. Implementation of hyperparameters optimization

Based on a available datasets, the hyperparameters can be optimized by the above framework. Before this, the hyperparameters domain, measures, and formulation should be implemented.

4.1 Design synthesis and post-processing

The dataset used for MLA training can often be generated by the design of experiment (DoE). Many algorithms are available to create DoE, e.g. Pseudo-Monte Carlo Sampling (PMCS), Latin Hypercube Sampling (LHS), and Orthogonal Array Sampling (OAS) [70]. In this study, the uniform LHS is used since it could fill the design space uniformly to fully explore the design space.

The size of the training dataset must be sufficiently large to ensure convergence and modeling accuracy. Yang et al (2005) [71] and Shi et al (2012) [10] determined the $3V_N$ is the minimum sample size to train a good surrogate model, where V_N is the number of design variables. Xu et al (2016) [72] developed a polynomial coefficient metric to evaluate the adequacy of sample size. Based on their theory, 1,000 data points are considered enough in the present case.

It is also noted that design variables may have different orders of magnitudes. This would outweigh features with a larger value over these with smaller value [73]. Therefore, the min-max normalization is used to scale the values of design variables into the same range $[0, 1]$ by

$$NV = \frac{v - v_{\min}}{v_{\max} - v_{\min}}, \quad (15)$$

where, for a specific variable, the NV is the normalized value, v is the variable value; v_{\max} and v_{\min} are the maximum and minimum value of this variable, respectively.

4.2 Hyperparameters domains

For each MLA, hyperparameters are identified for optimization considering their significant impact on model accuracy. Their initial values and ranges are determined based on the experience and previous studies as presented in Table 2. For GPR, the kernels and related parameters are tuned as the bold parameters in Equation 16,

$$\text{Kernels: } \begin{cases} \text{rbfdot (radial basis):} & k(x, x') = \exp(-\sigma \|x - x'\|^2) \\ \text{polydot (polynomial):} & k(x, x') = (\text{scale} \langle x, x' \rangle + \text{offset})^{\text{deg}} \\ \text{tanhdot (hyperbolic tangent):} & k(x, x') = \tanh(\text{scale} \langle x, x' \rangle + \text{offset}) \\ \text{laplacedot (Laplacian):} & k(x, x') = \exp(-\sigma \|x - x'\|) \end{cases}, \quad (16)$$

where, $\|x - x'\|$ is the Euclidean distance of vector x and x' ; **scale** and **offset** are used to scale the result of $\langle x, x' \rangle$ and add an offset, respectively. **deg** defines the degree of the polynomial kernel. σ is the weight of new nodes to the training nodes. The kernel function determines the ability to model the complexity and nonlinearity of the structural problem.

Besides kernel parameters, the ε and the weight factor C in Equations 8 and 9 are also tuned for SVM. A smaller ε will add more items to the latter term in Equation 8 and larger C will overweight error terms, which may cause the highly complex objective function. These may reach a highly accurate SVM model, but take the risk of overfitting since the relative underweighting of the former term in Equation 8 may cause a too complex model and so versa. The HOpt aims to gain the trade-off between model complexity and accuracy.

In RFR, the number of regression trees is a key factor for accuracy, but it is also critical to the computational cost. With more trees included, a higher computational cost will be caused. Meanwhile, the

tree-related parameters are also optimized, i.e. the number of randomly selected features for each split (NF), minimum terminal node size (Min TS) and maximum numbers of terminal nodes (Max TN).

Table 2 Hyperparameters of four MLAs with their initial values for the benchmark models and tuning space for optimization

MLA	Items	Hyperparameters						
GPR		Kernels			σ	Degree	scale	offset
	Initial value	rbfdot			0.5	--	--	--
	Range	<rbfdot, polydot, tanhdot, laplacedot>			[0 10] ^{*a}	1:10 ^{*b}	[0 10]	[-10 10]
SVM		C	ε	Kernels	σ	Degree	scale	offset
	Initial value	1	0.1	rbfdot	0.5	--	--	--
	Range	[0 10]	[0 1]	<rbfdot, polydot, tanhdot, laplacedot> ^{*c}	[0 10]	1:10	[0 10]	[-10 10]
RFR		Trees	NF	Min TS		Max TN		
	Initial value	500	3	5		Null ^{*d}		
	Range	1:1,000	1:100	1:50		1:1,000		
ANN		Hidden neurons	Activation	Optimizer	Batch size	Learning rate		Momentum
	Initial value	1	tanhdot	sgd	120	0.1		0.0
	Range	1:100	<tanhdot, relu, sigmoid, softrelu>	<sgd, rmsprop, adam, adagrad>	50:200	[0.01 1.0]		[0.5 0.99]

Note: ^{*a} [1 10] means the continuous variables with a range from 1 to 10; ^{*b} 1:10 means the integer variable with values from 1 to 10; ^{*c} <rbfdot, polydot, tanhdot, laplacedot> represents a categorical variable with four options available in the curly braces. ^{*d} Null means there is no limitation for this hyperparameter and depends on the requirements of other hyperparameters.

For ANN, one hidden layer is sufficient for general structural problems. The ANN structure and training related parameters are selected for optimization, that is, the number of hidden neurons, mini-batch sizes, activation functions, optimizers, learning rate, and momentum, where the momentum is only applicable to the *sgd* optimizer. ANN training aims to optimize weights for a predefined architecture. To increase this number may improve the accuracy but take the risk of overfitting. The mini-batch method trains ANN with a randomly selected portion of training dataset, which divides the training dataset into several subsets, and each will be used to train the ANN in sequence within a single epoch. This speeds up the convergence of the stochastic convex optimization but increases the training cost of a single epoch.

Optimizers determine the strategies to move towards the optimum. The *sgd* (stochastic gradient descent) updates weights in the form of

$$\mathbf{w}_{t+1} = \mathbf{w}_t - \zeta \cdot \nabla \mathbf{w}_t + \xi \cdot \Delta \mathbf{w}_{t-1}, \quad (17)$$

where \mathbf{w}_t and $\nabla \mathbf{w}_t$ are the weight matrix and gradient of the current epoch, respectively, and $\Delta \mathbf{w}_{t-1}$ is the step size of last epoch. ζ and ξ are the learning rate and momentum, respectively. A large learning rate accelerates the convergence speed but may lose the optimum while the too small value causes the high convergence cost. For other optimizers, adaptive learning rates are also used to speed up the learning process [67]. In this study, ANN training epochs were limited to 2,000, which is proven to be enough for training convergence by an additional test.

4.3 Measures of accuracy

During the surrogate modeling, a number of statistical indices, such as the root mean square error (RMSE), maximum absolute error (MXAE), mean absolute error, correlation, and decision coefficient, are frequently used as measures of accuracy [20, 74, 75]. In this study, the RMSE (Equation 18) and MXAE (Equation 19) are used as two HOpt objective measures [74] as the global and local accuracy measures, respectively.

$$RMSE = \sqrt{\frac{\sum_{i=1}^N (\tilde{f}(x^i) - f(x^i))^2}{N}}, \quad (18)$$

$$MXAE = \text{Max}(|\tilde{f}(x^i) - f(x^i)|) \quad (19)$$

where $\tilde{f}(x^i) - f(x^i)$ is the error of the predicted response relative to its real value of the i th design (x^i); N is the dataset size. Also, the training computational time (T) of MLAs is evaluated. This helps understand the effect of HOpt on the cost and make a decision on the selection of a suitable MLA in terms of computational cost.

4.4 Optimization formulation

Based on the hyperparameters and measures, the optimization problem is formulated in Equation 20. RMSE and MXAE are taken as the objectives of the HOpt. For each HOpt task of MLA, 30 initial designs are generated to construct the initial surrogate model. Another 70 evaluations (i.e. iterations, $N_T=100$) are

used to optimize the hyperparameters. The 5-folds cross-validation is used to train the model, which divides the training dataset into five subsets to train the model in iterations.

Find: \mathbf{x}_{hp}

Minimize: $RMSE$ and $MXAE$

$$\text{Subject to: } \begin{cases} \mathbf{x}_{hp_I} \in \min(\mathbf{x}_{hp_I}) : \max(\mathbf{x}_{hp_I}) \\ \min(\mathbf{x}_{hp_C}) \leq \mathbf{x}_{hp_C} \leq \max(\mathbf{x}_{hp_C}) \\ \mathbf{x}_{hp_Ca} \in \langle \mathbf{x}_{hp_Ca}^1, \mathbf{x}_{hp_Ca}^2, \dots, \mathbf{x}_{hp_Ca}^{NCa} \rangle \end{cases} \quad (20)$$

where \mathbf{x}_{hp_I} \mathbf{x}_{hp_C} \mathbf{x}_{hp_Ca} are the integral, continuous and categorical variables, respectively. Their domains, possible values or ranges, have been defined in Table 2. The datasets generated by DoE are used for MLAs training since the final aim is to construct surrogate models that predict the structural response(s) accurately.

5. Benchmark problems for the study of MLAs

In this study, four representative engineering structures are taken as examples to demonstrate the effect of hyperparameters by the HOpt. In these four problems, the variation of geometry (bar, sheet, and block), loading (static vs. dynamic) and boundary conditions (fully constrained and contact), as well as deformation modes (small vs. large deformation) are all considered. Hence, the methods and results associated with these case studies can be easily extended to a wide range of structures.

5.1 Structures subject to static loading

Under the static loading condition, two typical structures, i.e. a ten-bar planer truss (TbPT) [33] and a torque arm (TqA) [76-79], are introduced in Figure 4, since they are frequently taken as examples to verify structural design algorithms. In the TbPT model, the circular cross-section areas are taken as design variables with the range from 0.6 to 225.8 cm² and the other sizes are listed in Figure 4(a). Two loads with the same magnitude (444.8 kN) are applied on joints T and S. The *vertical displacement* (d) of joint S is taken as the response of this system, which is constrained within 60 cm in case the failure risk caused by the too-small cross-section areas.

To design the TqA structure, geometric constraints must be considered. The constant thickness of this structure is 3 mm and the distance between two circle centers is 420 mm. The design variables and their ranges are listed in Table 3. The left circle is fully constrained and loads are added to the right circle as

shown in Figure 4(b). To avoid structure failure, the stress is limited under 800 MPa and the *total mass* is used as the objective.

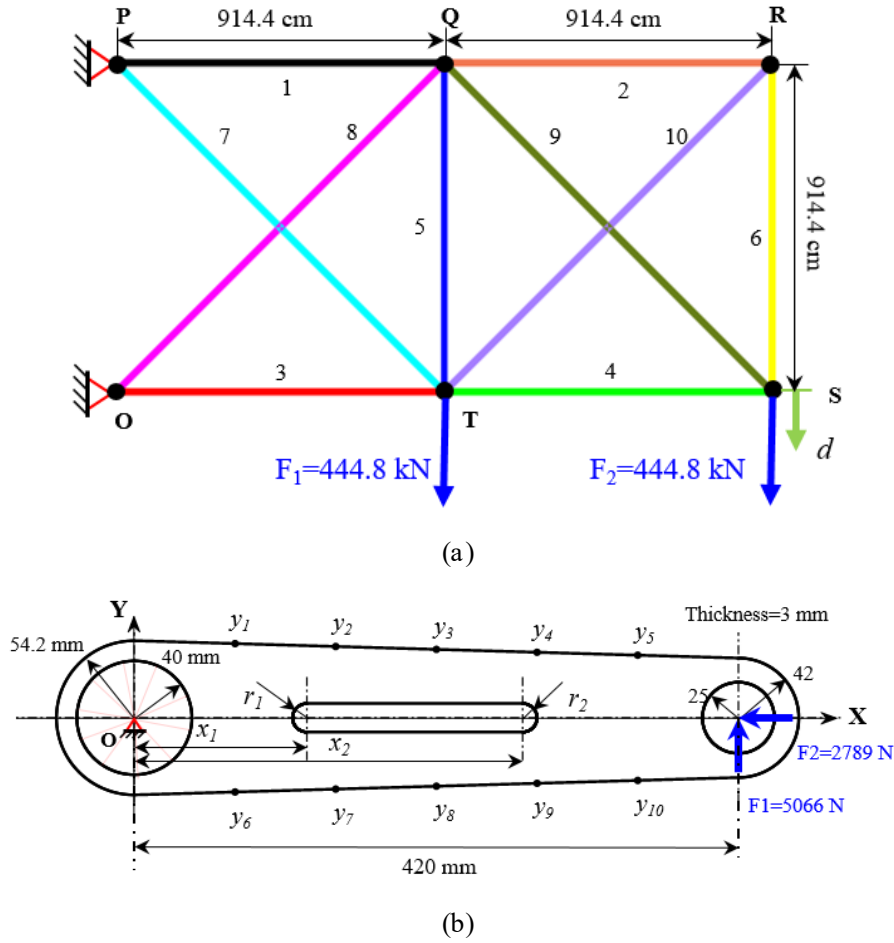


Figure 4 Two structures under static loading: (a) TbPT and (b) TqA

Table 3 Design variables and their ranges for the TqA structure

Design variable	Initial value /mm	Range/mm	Design variable	Initial value /mm	Range/mm
y_1	52	(30, 62)	y_8	48	(22, 58)
y_2	50	(26, 60)	y_9	46	(18, 56)
y_3	48	(22, 58)	y_{10}	44	(14, 54)
y_4	46	(18, 56)	x_1	120	(60, 200)
y_5	44	(14, 54)	x_2	270	(110, 395)
y_6	52	(30, 62)	r_1	10	(10, 40)
y_7	50	(26, 60)	r_2	10	(5, 40)

5.2 Structures subject to dynamic loading

Under the dynamic loading conditions, two vehicular components are studied, i.e. the thin-walled S-shaped beam (ShB) discussed in our previous studies [80, 81] and thin-walled octagonal multi-cell tube (OMcT) reported in Bai et al [82]. Their geometry parameterization and FE models are illustrated in Figure 5. As critical energy-absorbing parts on the passenger car, these structures can sustain large plastic deformation and dissipate a large amount of kinetic energy due to impact.

In Figure 5(a), the shape of ShB is fully described by 7 design variables and its total length is 1,000 mm. Figure 5(a) also shows the FE model of ShB, which is subjected to the frontal impact at 10 m/s. The specific energy absorption (SEA) is set as the design objective in Equation 21,

$$SEA = \frac{\int_0^d F(x)dx}{M}, \quad (21)$$

where M is the structural mass; $F(x)$ and d are the impact force-displacement history and total deflection, respectively.

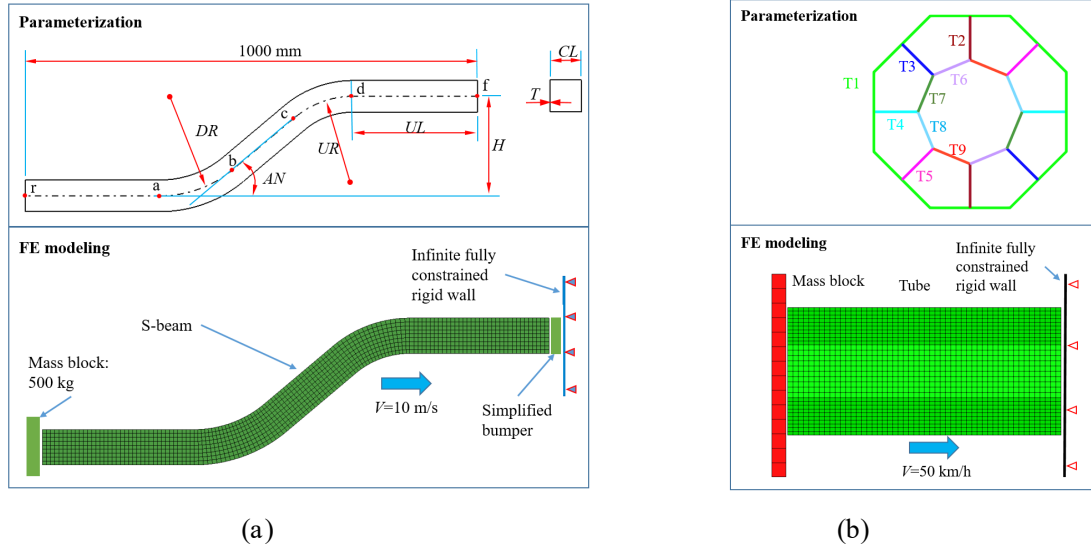


Figure 5 Two structures under dynamic loading: (a) the vehicle frontal S-shaped side beam (ShB) and (b) the octagonal multi-cell tube (OMcT), together with design variables and FE models

In the OMcT model, the cross-section is composed of the inner and outer octagons with ribs. The edge sizes of inner and outer octagons are 30 and 60 mm, respectively. The total length of OMcT is 310 mm. Different colors in Figure 5(b) represent different thicknesses. Each thickness is considered as one design variable and therefore, there are 9 design variables in total. The OMcT FE model impacts a fully

constrained rigid wall (velocity: 30 km/h) with the rear end attached to a mass block (600 kg) to represent the vehicle inertia effect. The coefficient force efficiency (CFE) is calculated as the response to assess the energy-absorbing efficiency in Equation 22,

$$CFE = \frac{\int_0^d F(x)dx}{d \times F_{\max}}, \quad (22)$$

where $\int_0^d F(x)dx/d$ is the averaged crushing force and F_{\max} is the peak crushing force. The detailed material parameters, loading, and boundary conditions can be seen in [80, 81]. These two models were validated in these studies and the details are not repeated here. In the current study, the impact speed of OMCT is increased to 50 km/h to represent the loading condition defined in NCAP standard (National Highway Traffic Safety Administration: <https://www.nhtsa.gov/laws-regulations>). The four models were simulated by the FE simulation using implicit (TbPT and TqA) and explicit (ShB and OMCT) solvers. For each structure, 1000 design cases are generated for MLA learning.

6. Results

6.1 Pareto front of hyperparameters

The Pareto fronts are generated through the SMBO as shown in the supplement file. Although the optimal hyperparameters may vary for different datasets, the values of hyperparameters in Pareto front would be close for the datasets with similar sample sizes and design space dimensions [24, 83]. In other words, the optimal hyperparameter values obtained from this study can be applied to the other similar design problems without significant change or used as the basis for optimization [23]. For each Pareto front, one hyperparameters group is selected randomly as summarized in Table 4, where corresponding mean loss values of five cross-validations are also included.

Table 4 Selected optimal hyperparameters for ML models with respect to the four structural datasets

MLA	Models	Hyperparameters							Loss	
GPR		Kernels	σ	Degree	scale	offset			RMSE	MXAE
	TbPT	polydot	NA	3	7.22	-2.24			0.0603	0.3786
	TqA	polydot	NA	2	1.73	1.07			0.0517	0.4594
	ShB	polydot	NA	3	2.30	1.08			0.0413	0.2341
	OMCT	polydot	NA	3	7.67	9.30			0.0551	0.2191

SVM		C	ε	Kernels	σ	Degree	scale	offset	RMSE	MXAE
	TbPT	0.81	0.07	polydot	NA	7	2.73	5.87	0.0626	0.3777
	TqA	2.81	0.41	polydot	NA	1	4.03	-2.09	0.0545	0.4953
	ShB	9.77	0.13	laplacedot	0.37	NA	NA	NA	0.0466	0.3238
	OMcT	9.20	0.05	polydot	NA	2	9.25	2.96	0.0730	0.2576
RFR		Trees	NF	Min TS		Max TN		RMSE	MXAE	
	TbPT	773	10	1		304		0.0463	0.4169	
	TqA	569	9	1		682		0.0953	0.4414	
	ShB	718	7	1		1,000		0.0454	0.2975	
	OMcT	879	9	1		493		0.0795	0.3768	
ANN		Hidden neurons	Activ- ation	Optimizer	Batch size	Learning rate	Momentum	RMSE	MXAE	
	TbPT	26	relu	sgd	199	0.77	0.83	0.0473	0.2945	
	TqA	19	relu	adagrad	108	0.57	NA	0.0506	0.4503	
	ShB	8	tanhdot	adagrad	85	0.30	NA	0.0405	0.2571	
	OMcT	36	tanhdot	sgd	98	0.97	0.92	0.0421	0.1585	

6.2 Effect of hyperparameters optimization

By using the values in Table 4, sixteen models are trained with 5-folds cross-validation. The distributions of RMSE and MXAE among 5-folds cross-validation are presented by boxplots in Figure 6 and 7, respectively. The results before (trained using initial values in Table 2) and after the HOpt are compared. The median is represented by the black line in the boxes. A lower median value indicates a higher median prediction accuracy. The upper and lower bounds of the box represent the interquartile range with the 25th percentile lower and 75th percentile upper limits. The distance between the upper and lower bounds measures the robustness of the model. Smaller distance indicates higher robustness. For points outside the range of the upper and lower bounds of whiskers are outliers.

As shown in Figure 6 and Figure 7, HOpt reduces the median of the RMSE and MXAE values, which indicate improving the prediction accuracy, in most case studies. The improvements in accuracy are particularly significant in TbPT and ShB. However, HOpt leads to less improvement in the case of TqA due to the high complexity of the problem. Similar trends can be observed in model robustness. HOpt can

improve the robustness of the MLA models in most cases. However, exceptions can be observed in TqA and OMcT, where the robustnesses of GPR, SVM, and RFR deteriorates after HOpt.

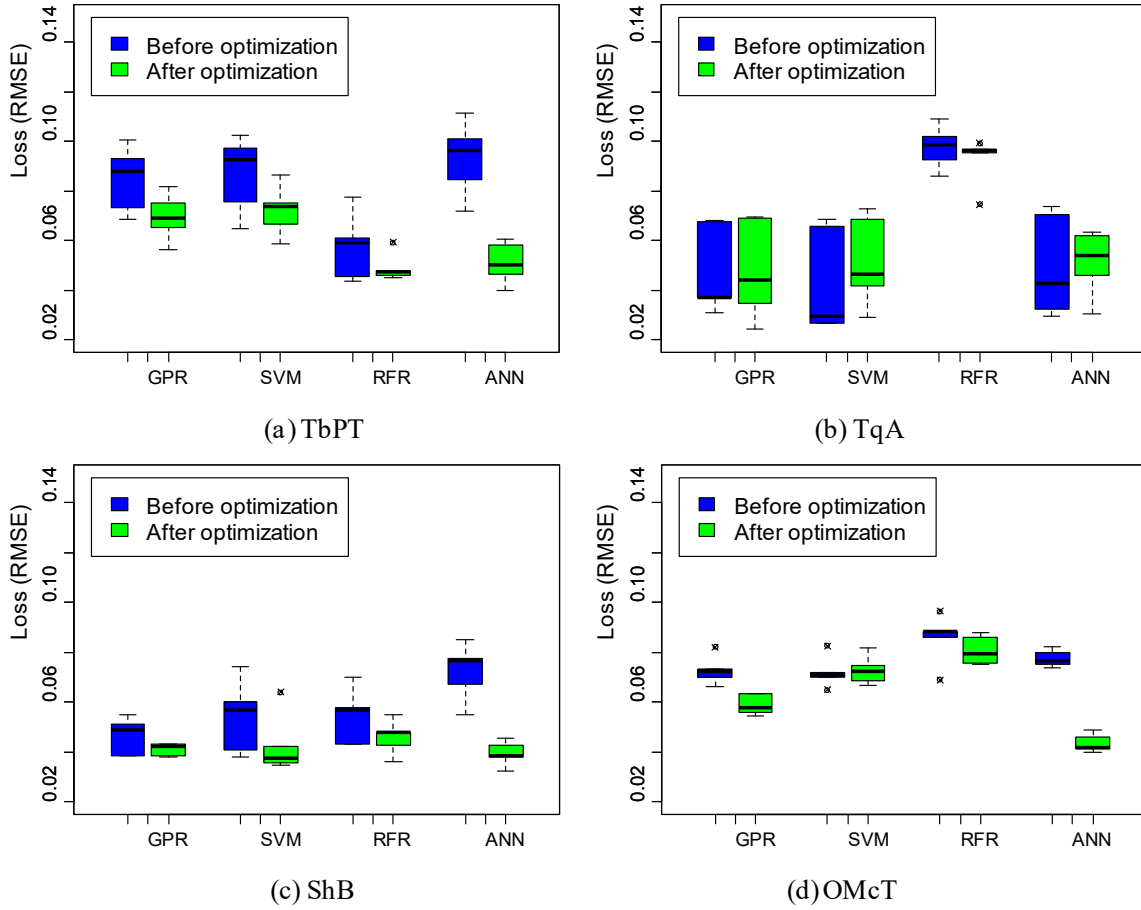
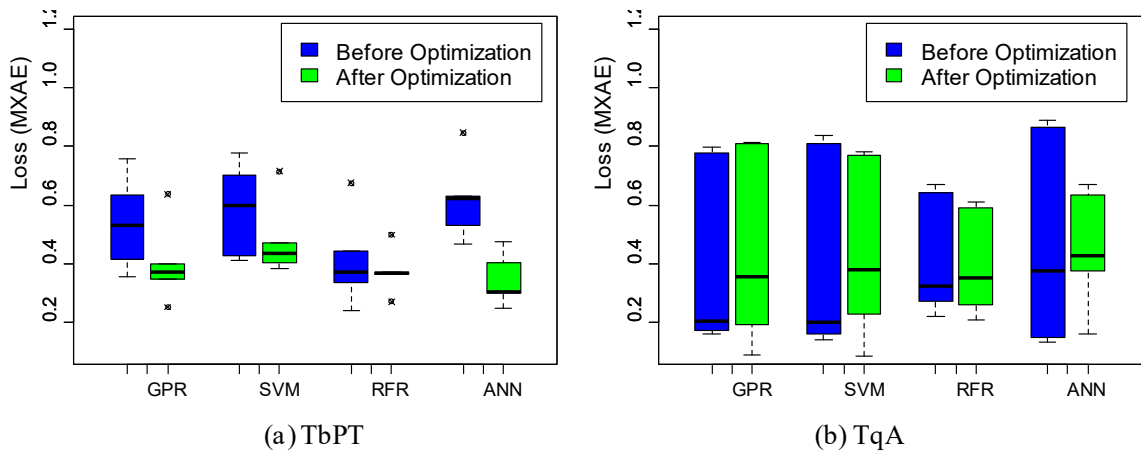


Figure 6 Comparison of the RMSE accuracy of the four MLAs trained by the four structural datasets before and after HOpt



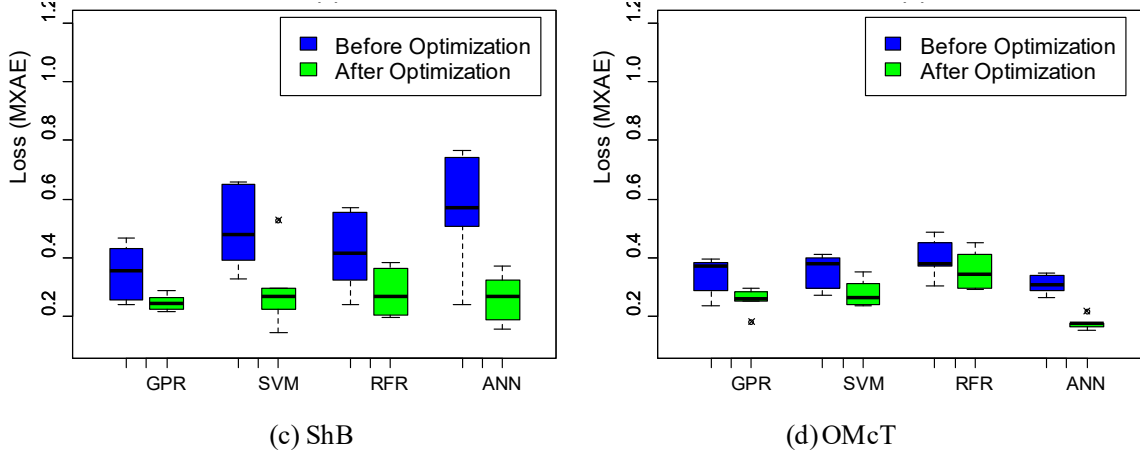


Figure 7 Comparison of the MXAE accuracy of the four MLAs trained by the four structure datasets before and after HOpt

6.3 Computational time evaluation

By comparing the time of a single training before and after the HOpt, the impact of HOpt on computational cost is evaluated. The computational power is as follows: Dell Precision Tower 5810 with Intel Xeon CPU E5-2690 v3: 2.6 GHz turbo up to 3.5 GHz and 32 GB RAM. Figure 8 shows the computational time of the four MLAs trained by the four structural datasets before and after HOpt. The results indicate that there is almost no time cost change for GPR training since its hyperparameters have no influence on the model size and then, training task scale. According to Figure 8(d), however, the SVM training time is increased greatly for the OMcT. Regarding this model in Table 4, the large error penalization C (i.e. 9.2) gives a large weight to the error term in Equation 8. Meanwhile, the low value (i.e. 0.05) of ϵ -bounds causes more samples falling out of ϵ -bounds. Then, their error with respect to the ϵ -bounds are added into the error term, which increases the complexity of objective function and the difficulty to minimize errors. These lead to a high training cost.

The training time of RFR is the time used to evaluate the splitting nodes of all trees. In this way, the time of RFR training is closely related to the number of trees (Trees) and NF. Min TS and Max TN can also affect the number of non-leaf nodes, since they are related to the single tree scale and then the RFR model size. However, the degree of their influences to the final training time is less compared with the Trees and NF. A larger number of trees and more NF can improve prediction accuracy while they increase the model scale and then the training time.

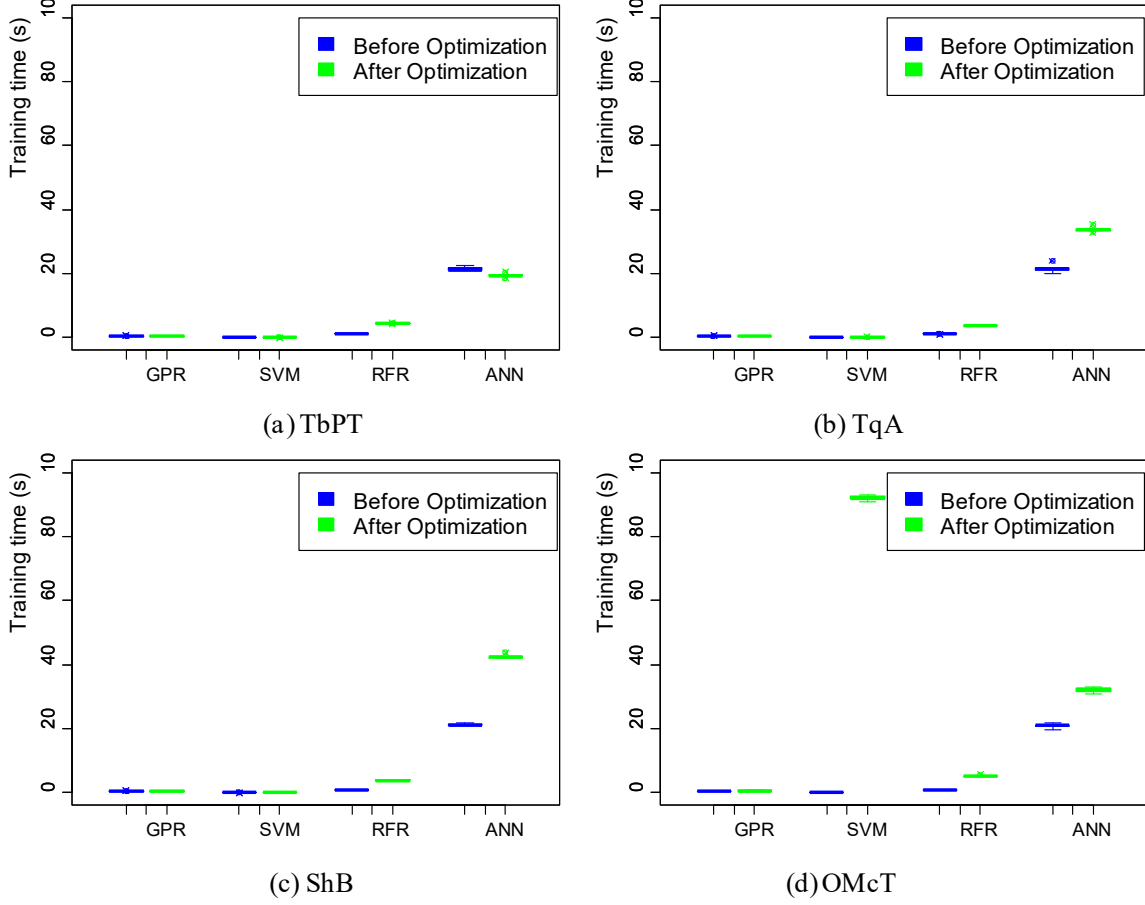


Figure 8 Training time comparison of the 16 models before and after HOpt

ANN training time is related to the combined effect of the mini-batch size, learning rate, and optimizer and so on. As indicated in Table 4 and Figure 8, after HOpt, the ANN trained by TbPT is reduced slightly, which is caused by the larger learning rate, which accelerates the training convergence. However, the other structural cases presented lower convergence speed although they have larger learning rates, which are caused by the smaller mini-batch sizes. This increases the number of batch training within a single epoch, which rises the training time of a single epoch but lowers the number of epochs for convergence. These suggest that the mini-batch size takes the primary effect on the training time and is followed by the learning rate under a fixed training epoch. The other hyperparameters are more related to model accuracy than the training cost.

In summary, compared with GPR and SVM, the training time of ANN and RFR is more sensitive to hyperparameter values. HOpt improved the ANN performance most significantly, which is followed by the GPR. Therefore, it is recommended to conduct HOpt for ANN if enough computational sources are

a available. Otherwise, the GPR is recommended for applying the HOpt. Besides, in the HOpt for SVM, small ε -bounds or large error penalization C should be avoided, because they will cause a too complex training objective function and then unexpected singularities and a high convergence cost.

7. Discussion

In this section, an analysis is carried out on the relationship between the performance of HOpt method to improve the MLA modeling performance and characteristics of the design problems, as summarized in Table 5. The characteristics include the structure type, the types and number of design variables, load type, and the design domain continuity, which performances are mainly RMSE, MXAE and computational time. Previous studies have demonstrated that the dimensionality and nonlinearity of design problems, which partially depends on the structure and load types, have a strong impact on the surrogate model accuracy and robustness [19, 84]. In addition to structure and load types, the dimensionality of the design space, continuity of the feasible domain, and the design variable type also influence the complexity of the problem. Due to the design constraints, the feasible domains of TbPT and TqA are broken into discontinuous subdomains. The nonlinear boundaries of discontinuous feasible domains pose an additional level of challenge to MLA model training. Furthermore, mixed-variable problems are more challenging for MLA models.

In Table 5, the improvement in accuracy (mean) and robustness (SD) of each MLA model after HOpt are listed for each benchmark problem. The improvement is presented as the percentage of reduction in the values of mean and SD values, where the minus values indicate the reduction of measures and improvement and so versa. The reduction in training time is provided as well. The detailed values of each measure before and after HOpt are listed in the supplement file. In Table 5, the cases with no improvement are denoted with red and the increased training time is denoted with blue. With all the information on problem complexity and MLA performances, we discuss the effect of HOpt in the following three aspects.

- Effect of HOpt on MLA model accuracy

HOpt may not always improve the model accuracy for problems with characteristics similar to the TqA. Compared with the other three structures, the HOpt takes less and unstable improvement on the TqA. The SVM and ANN performance for TqA are even deteriorated slightly after HOpt. This was caused the mixed-variable design space and we also notice that this case study has the highest dimensionality in all

cases. More optimization cycles, as described in Section 3, may be helpful to gain more improvement. Also, the discontinuous design domain induced singular points on the boundaries, which will cause difficulties in training surrogate models. For example, it may cause the singularity in the covariance matrix of GPR as shown in Equation 6.

Table 5 The characteristics and HOpt performance of the four design benchmark structures

Category	Item		Structure			
			TbPT	TqA	ShB	OMcT
Complexity matrix	Structure type		Truss	Block	Thin-wall	Thin-wall
	No. of variables		10	14	7	9
	Variables type ^{*a}		Single	Mixed	Mixed	Single
	Load type		Static	Static	Impact	Impact
	Design domain ^{*b}		Discontinuous	Discontinuous	Continuous	Continuous
MLA	Measure		Reduction by % after HOpt ('-' indicates measure reduction or improvement)			
GPR	RMSE	Mean	-18.8	0.0	-10.9	-19.2
		SD	-30.8	11.1	-75.0	-33.3
	MXAE	Mean	-25.6	7.1	-29.2	-23.9
		SD	-12.3	2.7	-70.3	-34.8
	Time/s	Mean	-19.5	-21.2	-15.8	17.0
SVM	RMSE	Mean	-16.3	18.6	-20.4	0.0
		SD	-37.5	-18.2	-20.0	-16.7
	MXAE	Mean	-17.5	4.0	-41.9	-20.5
		SD	-16.7	-12.2	-5.3	-20.3
	Time/s	Mean	-37.0	233.3	-8.0	143931.3
RFR	RMSE	Mean	-14.0	-5.2	-14.8	-5.8
		SD	-57.1	11.1	-36.4	-40.0
	MXAE	Mean	-9.4	-4.9	-32.5	-10.1
		SD	-50.3	-13.6	-39.6	-2.8
	Time/s	Mean	299.8	222.8	398.7	491.8
ANN	RMSE	Mean	-45.2	2.0	-45.8	-44.2
		SD	-46.7	-38.1	-54.5	0.0
	MXAE	Mean	-44.1	-6.2	-53.5	-42.7
		SD	-36.8	-44.5	-57.5	-29.4
	Time/s	Mean	-9.5	55.4	98.5	53.2

Note: ^{*a} Type of variables: "Single" indicates that only one type of design variables is contained, for example, the nine thickness variables of OMcT. "Mixed" indicates that multiple types of design variables are contained, for example, the radius, length, and node location variables of TqA. ^{*b} Design domain (continuity): continuous or discontinuous.

- Effect of HOpt on MLA model robustness

HOpt improves the robustness of MLA models in the design problems with an intermediate complexity (TbPT and ShB). For the simplest problem (OMcT), HOpt is also helpful, but the improvement is less significant because MLA models already achieve good robustness without HOpt. It should be noted that HOpt may reduce model robustness in a relatively complex design problem (e.g. TqA). This issue can be partially avoided by simplifying a complex problem through dimension reduction and eliminating mixed variables [85, 86].

- Effect of HOpt on MLA training cost

No clear trend can be observed in the relation between HOpt and the training cost. As discussed in Section 6.3, the training time is independent of the features of the design problem but related to the MLA model architecture. The knowledge of MLA model architecture could help estimate and reduce the training time of MLA and the associated HOpt.

To summarize based on the results of present study, HOpt may lead to deteriorated accuracy and robustness for design problems with the relatively high complexity, but it can improve the modeling performance with less design variables. However, further reduction of the dimension will eliminate the need of HOpt. We recommend GPR as a good start for complex problems due to its low training cost and relatively high accuracy. It is also noticed that HOpt leads to insignificant improvement in simple design problems.

Conclusions

In this study, the effects of hyperparameters on MLA surrogate models, namely GPR, SVM, RFR, and ANN are analyzed in detail. A HOpt framework is proposed for optimizing the hyperparameter values to improve model accuracy and robustness. By applying the surrogate modeling and HOpt methods to four benchmark examples, we investigated the impact of HOpt on the accuracy, robustness, and computational costs of the surrogate models.

In general, the HOpt performs better for the MLA model when handling a design problem with intermediate complexity. HOpt may deteriorate the model accuracy and robustness in problems with mixed variables and relative higher dimensional design space. Besides, the HOpt has less impact on the relatively simple problem, which can be well modeled without HOpt. Therefore, the HOpt is recommended for the

design problems with an intermediate degree of complexity. The HOpt may improve the MLA modeling performance for complex problems by reducing the dimension or using more HOpt iterations. GPR is recommended with HOpt due to its low training cost and relatively high accuracy.

The training costs before and after hyperparameters tuning are also evaluated through a single training process. Followed by the RFR, the training time of ANN exhibits the highest sensitivity to the HOpt. ANN training cost is closely related to the learning rate and mini-batch size. The mini-batch size could speed up the convergence and reduce the iteration cost. The RFR training cost is linearly related to the scale of forest (i.e. the number of trees and each tree's nodes). GPR and SVM are insensitive to the hyperparameters tuning. A high computational cost for SVM may occur under the condition of the narrow ε -bounds and the high weight (C) of the error term, which should be avoided.

A parametric study conducted on the hyperparameters' influence on RMSE and MXAE is discussed in the supplement file. The results indicate that the polynomial and Laplacian kernels are recommended for the GPR for a high modeling accuracy. The low degree (2 or 3) of the polynomial kernel and low sigma of Laplacian kernel are the good choices for the SVM-based surrogate modeling. Meanwhile, The ANN trained with the *tanh* or *relu* activation functions using *sgd* or *adagrad* optimizers shows a good performance.

Acknowledgements

The first author would like to thank ERAU for the partial financial support through the FIRST grant and Ph.D. program, and the Cooperative Internship Program provided by University of Connecticut and Embry-Riddle Aeronautical University.

Conflict of Interest

The authors declare that they have no conflict of interest.

References

- [1] Boursier Niutta, C., et al., Surrogate modeling in design optimization of structures with discontinuous responses. Structural and Multidisciplinary Optimization, 2018. 57(5): p. 1857-1869.
- [2] Du, X. and F. Zhu, A new data-driven design methodology for mechanical systems with high dimensional design variables. Advances in Engineering Software, 2018. 117(2017): p. 18-28.

- [3] Du, X., et al., Modeling the motion of small unmanned aerial system (sUAS) due to ground collision. Proceedings of the Institution of Mechanical Engineers, Part G: Journal of Aerospace Engineering, 2018. 232(10): p. 1961-1970.
- [4] Els, P.S., et al., The ride comfort vs. handling compromise for off-road vehicles. Journal of Terramechanics, 2007. 44(4): p. 303-317.
- [5] Fang, J., et al., On design optimization for structural crashworthiness and its state of the art. Structural and Multidisciplinary Optimization, 2017. 55(3): p. 1091-1119.
- [6] Fan, X., P. Wang, and F. Hao, Reliability-based design optimization of crane bridges using Kriging-based surrogate models. Structural and Multidisciplinary Optimization, 2019. 59(3): p. 993-1005.
- [7] Ozcanan, S. and A.O. Atahan, RBF surrogate model and EN1317 collision safety-based optimization of two guardrails. Structural and Multidisciplinary Optimization, 2019: p. 1-20.
- [8] Ben Salem, M. and L. Tomaso, Automatic selection for general surrogate models. Structural and Multidisciplinary Optimization, 2018. 58(2): p. 719-734.
- [9] Zhou, X. and T. Jiang, Metamodel selection based on stepwise regression. Structural and Multidisciplinary Optimization, 2016. 54(3): p. 641-657.
- [10] Shi, L., R.J. Yang, and P. Zhu, A method for selecting surrogate models in crashworthiness optimization. Structural and Multidisciplinary Optimization, 2012. 46(2): p. 159-170.
- [11] Yin, H., et al., On the ensemble of metamodels with multiple regional optimized weight factors. Structural and Multidisciplinary Optimization, 2018. 58(1): p. 245-263.
- [12] Ferreira, W.G. and A.L. Serpa, Ensemble of metamodels: extensions of the least squares approach to efficient global optimization. Structural and Multidisciplinary Optimization, 2017. 57(1): p. 131-159.
- [13] Ferreira, W.G. and A.L. Serpa, Ensemble of metamodels: the augmented least squares approach. Structural and Multidisciplinary Optimization, 2015. 53(5): p. 1019-1046.
- [14] Acar, E. and K. Solanki, Improving the accuracy of vehicle crashworthiness response predictions using an ensemble of metamodels AU - Acar, Erdem. International Journal of Crashworthiness, 2009. 14(1): p. 49-61.
- [15] Acar, E. and M. Rais-Rohani, Ensemble of metamodels with optimized weight factors. Structural and Multidisciplinary Optimization, 2009. 37(3): p. 279-294.
- [16] Mehmani, A., et al., Concurrent surrogate model selection (COSMOS): optimizing model type, kernel function, and hyper-parameters. Structural and Multidisciplinary Optimization, 2017. 57(3): p. 1093-1114.
- [17] Díaz-Manríquez, A., G. Toscano-Pulido, and W. Gómez-Flores. On the selection of surrogate models in evolutionary optimization algorithms. in Evolutionary Computation (CEC), 2011 IEEE Congress on. 2011. IEEE.

- [18] Couckuyt, I., et al. Automatic surrogate model type selection during the optimization of expensive black-box problems. in Simulation Conference (WSC), Proceedings of the 2011 Winter. 2011. IEEE.
- [19] Jin, R., W. Chen, and T.W. Simpson, Comparative studies of metamodeling techniques under multiple modelling criteria. Structural and multidisciplinary optimization, 2001. 23(1): p. 1-13.
- [20] Zhao, D. and D. Xue, A comparative study of metamodeling methods considering sample quality merits. Structural and Multidisciplinary Optimization, 2010. 42(6): p. 923-938.
- [21] Hutter, F., H.H. Hoos, and K. Leyton-Brown. Sequential model-based optimization for general algorithm configuration. in International Conference on Learning and Intelligent Optimization. 2011. Springer.
- [22] Snoek, J., H. Larochelle, and R.P. Adams. Practical bayesian optimization of machine learning algorithms. in Advances in neural information processing systems. 2012.
- [23] Bardenet, R., et al. Collaborative hyperparameter tuning. in International Conference on Machine Learning. 2013.
- [24] Yogatama, D. and G. Mann, Efficient Transfer Learning Method for Automatic Hyperparameter Tuning. Artificial Intelligence and Statistics, 2014: p. 1077-1085.
- [25] Klein, A., et al., Fast Bayesian Optimization of Machine Learning Hyperparameters on Large Datasets. arXiv preprint 2016. arXiv:1605.07079.
- [26] Song, X., et al., Crashworthiness optimization of foam-filled tapered thin-walled structure using multiple surrogate models. Structural and Multidisciplinary Optimization, 2012. 47(2): p. 221-231.
- [27] Xiong, F., et al., Multi-objective lightweight and crashworthiness optimization for the side structure of an automobile body. Structural and Multidisciplinary Optimization, 2018.
- [28] Pan, F., P. Zhu, and Y. Zhang, Metamodel-based lightweight design of B-pillar with TWB structure via support vector regression. Computers & Structures, 2010. 88(1): p. 36-44.
- [29] Zhu, P., et al., Use of support vector regression in structural optimization: Application to vehicle crashworthiness design. Mathematics and Computers in Simulation, 2012. 86: p. 21-31.
- [30] Garijo, N., et al., Computational evaluation of different numerical tools for the prediction of proximal femur loads from bone morphology. Computer Methods in Applied Mechanics and Engineering, 2014. 268: p. 437-450.
- [31] Mannodi-Kanakkithodi, A., G. Pilania, and R. Ramprasad, Critical assessment of regression-based machine learning methods for polymer dielectrics. Computational Materials Science, 2016. 125: p. 123-135.
- [32] Rodriguez-Galiano, V., et al., Machine learning predictive models for mineral prospectivity: An evaluation of neural networks, random forest, regression trees and support vector machines. Ore Geology Reviews, 2015. 71: p. 804-818.

- [33] Lee, S., et al., Background Information of Deep Learning for Structural Engineering. Archives of Computational Methods in Engineering, 2017. 25(1): p. 121-129.
- [34] Bergstra, J.S., et al. Algorithms for hyper-parameter optimization. in Advances in neural information processing systems. 2011.
- [35] Mukherjee, A. and J.M. Deshpande, Application of Artificial Neural Networks in Structural Design Expert-Systems. Computers & Structures, 1995. 54(3): p. 367-375.
- [36] Kapania, R.K. and Y. Liu, Applications of artificial neural networks in structural engineering with emphasis on continuum models. 1998.
- [37] Nagendra, S., et al., Optimal rapid multidisciplinary response networks: RAPIDDISK. Structural and Multidisciplinary Optimization, 2004. 29(3): p. 213-231.
- [38] Lee, J., H. Jeong, and S. Kang, Derivative and GA-based methods in metamodeling of back-propagation neural networks for constrained approximate optimization. Structural and Multidisciplinary Optimization, 2007. 35(1): p. 29-40.
- [39] Tang, Y.C. and J. Chen, Robust design of sheet metal forming process based on adaptive importance sampling. Structural and Multidisciplinary Optimization, 2009. 39(5): p. 531-544.
- [40] Guo, Z. and G. Bai, Application of least squares support vector machine for regression to reliability analysis. Chinese Journal of Aeronautics, 2009. 22(2): p. 160-166.
- [41] Wang, H., E. Li, and G.Y. Li, Probability-based least square support vector regression metamodeling technique for crashworthiness optimization problems. Computational Mechanics, 2010. 47(3): p. 251-263.
- [42] Huang, Z., et al., Optimal design of aeroengine turbine disc based on kriging surrogate models. Computers & Structures, 2011. 89(1): p. 27-37.
- [43] Zhang, Y., et al., Optimization of foam-filled bitubal structures for crashworthiness criteria. Materials & Design, 2012. 38: p. 99-109.
- [44] Haleem, K. and A. Gan, Effect of driver's age and side of impact on crash severity along urban freeways: A mixed logit approach. Journal of Safety Research, 2013. 46: p. 67-76.
- [45] Song, X., et al., Crashworthiness optimization of foam-filled tapered thin-walled structure using multiple surrogate models. Structural and Multidisciplinary Optimization, 2013. 47(2): p. 221-231.
- [46] Yin, H., et al., Crashworthiness optimization design for foam-filled multi-cell thin-walled structures. Thin-Walled Structures, 2014. 75: p. 8-17.
- [47] Lukaszewicz, D., et al. A Design and Analysis Method for Automotive and Aerospace Composite Structures including Manufacturing Variations. in Proc. of the American Society for Composites 29th Conference. 2014.

- [48] Lukaszewicz, D. and B. AG. A Design Method for Robust Automotive and Aerospace Composite Structures Including Manufacturing Variations. in 24th International Technical Conference on the Enhanced Safety of Vehicles (ESV) National Highway Traffic Safety Administration. 2015.
- [49] Rodriguez-Galiano, V., M. Chica-Olmo, and M. Chica-Rivas, Predictive modelling of gold potential with the integration of multisource information based on random forest: a case study on the Rodalquilar area, Southern Spain AU - Rodriguez-Galiano, V.F. International Journal of Geographical Information Science, 2014. 28(7): p. 1336-1354.
- [50] Fang, J., et al., Crashworthiness design of foam-filled bitubal structures with uncertainty. International Journal of Non-Linear Mechanics, 2014. 67: p. 120-132.
- [51] Fang, J., et al., On design of multi-cell tubes under axial and oblique impact loads. Thin-Walled Structures, 2015. 95: p. 115-126.
- [52] Tang, Z., et al., Data-driven train set crash dynamics simulation. Vehicle System Dynamics, 2016. 55(2): p. 149-167.
- [53] Liu, X., et al., An adaptive local range sampling method for reliability-based design optimization using support vector machine and Kriging model. Structural and Multidisciplinary Optimization, 2016. 55(6): p. 2285-2304.
- [54] Yu, Y., et al., Deep learning for determining a near-optimal topological design without any iteration. Structural and Multidisciplinary Optimization, 2018.
- [55] Raihan, M., M. Hossain, and T. Hasan, Data mining in road crash analysis: the context of developing countries AU - Raihan, Md Asif. International Journal of Injury Control and Safety Promotion, 2018. 25(1): p. 41-52.
- [56] Duan, L., et al., Parametric modeling and multiobjective crashworthiness design optimization of a new front longitudinal beam. Structural and Multidisciplinary Optimization, 2018.
- [57] Palar, P.S. and K. Shimoyama, Efficient global optimization with ensemble and selection of kernel functions for engineering design. Structural and Multidisciplinary Optimization, 2018. 59(1): p. 93-116.
- [58] Gong, H., et al., Use of random forests regression for predicting IRI of asphalt pavements. Construction and Building Materials, 2018. 189: p. 890-897.
- [59] Fournier, E., S. Grihon, and T. Klein, A case study: Influence of Dimension Reduction on regression trees-based Algorithms-Predicting Aeronautics Loads of a Derivative Aircraft. arXiv preprint arXiv:1812.02310, 2018.
- [60] Richardson, R.R., M.A. Osborne, and D.A. Howey, Gaussian process regression for forecasting battery state of health. Journal of Power Sources, 2017. 357: p. 209-219.
- [61] Duvenaud, D., et al., Structure discovery in nonparametric regression through compositional kernel search. arXiv preprint arXiv:1302.4922, 2013.

- [62] Smola, A.J. and B. Scholkopf, A tutorial on support vector regression. *Statistics and Computing*, 2004. 14(3): p. 199-222.
- [63] Smola, A.J., B. Schölkopf, and K.-R. Müller. General cost functions for support vector regression. in *IN Proceedings of the 8th International Conference on Artificial Neural Networks*. 1998. Citeseer.
- [64] Vapnik, V., *The nature of statistical learning theory*. 2013: Springer science & business media.
- [65] Han, J., J. Pei, and M. Kamber, *Data mining: concepts and techniques*. 2011: Elsevier.
- [66] Breiman, L., Random forests. *Machine learning*, 2001. 45(1): p. 5-32.
- [67] Goodfellow, I., et al., *Deep learning*. Vol. 1. 2016: MIT press Cambridge.
- [68] Jones, D.R., M. Schonlau, and W.J. Welch, Efficient global optimization of expensive black-box functions. *Journal of Global optimization*, 1998. 13(4): p. 455-492.
- [69] Bischl, B., et al., mlrMBO: A modular framework for model-based optimization of expensive black-box functions. *arXiv preprint arXiv:1703.03373*, 2017.
- [70] Giunta, A., S. Wojtkiewicz, and M. Eldred. Overview of modern design of experiments methods for computational simulations. in *41st Aerospace Sciences Meeting and Exhibit*. 2003.
- [71] Yang, R., et al., Metamodeling development for vehicle frontal impact simulation. *Journal of Mechanical Design*, 2005. 127(5): p. 1014-1020.
- [72] Xu, H., C.-H. Chuang, and R.-J. Yang. Mixed-Variable Metamodeling Methods for Designing Multi-Material Structures. in *ASME 2016 International Design Engineering Technical Conferences and Computers and Information in Engineering Conference*. 2016. American Society of Mechanical Engineers.
- [73] Mohamad, I.B. and D. Usman, Standardization and its effects on K-means clustering algorithm. *Research Journal of Applied Sciences, Engineering and Technology*, 2013. 6(17): p. 3299-3303.
- [74] Zhang, J., S. Chowdhury, and A. Messac, An adaptive hybrid surrogate model. *Structural and Multidisciplinary Optimization*, 2012. 46(2): p. 223-238.
- [75] Chugh, T., et al., A survey on handling computationally expensive multiobjective optimization problems with evolutionary algorithms. *Soft Computing*, 2017.
- [76] Kim, N.H. and Y. Chang, Eulerian shape design sensitivity analysis and optimization with a fixed grid. *Computer Methods in Applied Mechanics and Engineering*, 2005. 194(30-33): p. 3291-3314.
- [77] Van Miegroet, L., Generalized shape optimization using XFEM and level set description. 2012, Université de Liège, Liège, Belgique.

- [78] Cai, S., et al., Stress constrained shape and topology optimization with fixed mesh: A B-spline finite cell method combined with level set function. *Computer Methods in Applied Mechanics and Engineering*, 2014. 278: p. 361-387.
- [79] Bennett, J.A. and M.E. Botkin, Structural shape optimization with geometric description and adaptive mesh refinement. *AIAA Journal*, 1985. 23(3): p. 458-464.
- [80] Du, X., F. Zhu, and C.C. Chou, A New Data-Driven Design Method for Thin-Walled Vehicular Structures Under Crash Loading. *SAE Int. J. Trans. Safety*, 2017. 5(2): p. 188-193.
- [81] Du, X. and F. Zhu, A new data-driven design methodology for mechanical systems with high dimensional design variables. *Advances in Engineering Software*, 2018. 117: p. 18-28.
- [82] Bai, Z., et al., Crashworthiness optimal design of a new extruded octagonal multi-cell tube under dynamic axial impact. *International Journal of Vehicle Safety*, 2018. 10(1): p. 40-57.
- [83] Brochu, E., T. Brochu, and N. de Freitas. A Bayesian interactive optimization approach to procedural animation design. in *Proceedings of the 2010 ACM SIGGRAPH/Eurographics Symposium on Computer Animation*. 2010. Eurographics Association.
- [84] Simpson, T.W., et al., Metamodels for computer-based engineering design: survey and recommendations. *Engineering with Computers*, 2001. 17(2): p. 129-150.
- [85] Du, X., A Data Mining Methodology for Vehicle Crashworthiness Design. 2019, Embry-Riddle Aeronautical University.
- [86] Du, X. and F. Zhu, A novel principal components analysis (PCA) method for energy absorbing structural design enhanced by data mining. *Advances in Engineering Software*, 2019. 127(2019): p. 17-27.

Supplementary material for:

Understanding the effect of hyperparameter optimization on machine learning models for structure design problems

Xianping Du¹⁺, Hongyi Xu², Feng Zhu^{1,3*}

1 Department of Mechanical Engineering, Embry-Riddle Aeronautical University, Daytona Beach, FL 32114, USA

2 Department of Mechanical Engineering, University of Connecticut, Storrs, CT 06269, USA

3 Hopkins Extreme Materials Institute and Department of Mechanical Engineering, Johns Hopkins University, Baltimore, MD, 21218, USA

Supplemental Material Section A:

This supplementary section includes the full table of Pareto fronts from the HOpt.

Supplemental Material Section B:

This supplementary section includes the hyperparameters effect analysis on the MLA model accuracy (RMSE) for the GPR and ANN based on the four benchmark structures

Supplemental Material Section C:

This supplementary section includes the characteristic analysis of the four benchmark problems and corresponding MLA performance before and after the HOpt.

⁺ Current affiliation: Department of Mechanical and Aerospace Engineering, Rutgers University, Piscataway, NJ 08854, USA

^{*} Corresponding author: Hopkins Extreme Materials Institute, Johns Hopkins University, 3400 N Charles St, Baltimore, MD 21218, USA

E-mail: fengzhume@gmail.com (Dr. Feng Zhu); Xianping Du (DUX1@mv.crau.edu); Hongyi Xu (hongyi.3.xu@uconn.edu)

Supplemental Material Section A:

Table A.1 All Pareto fronts obtained from the multi-objective HOpt and the frequencies of categorical hyperparameters, together with the average and S.D. of numerical hyperparameters for four structures

GPR		Kernel	σ	Degree	Scale	Offset			RMSE	MXAE	
	TbPT	polydot	NA	3	7.22	-2.24			0.0603	0.3786	
		polydot	NA	3	3.71	-2.24			0.0603	0.3786	
	TqA	polydot	NA	2	1.73	1.07			0.0517	0.4594	
		laplacedot	0.46	NA	NA	NA			0.0664	0.4189	
		laplacedot	0.34	NA	NA	NA			0.0597	0.4208	
		laplacedot	0.44	NA	NA	NA			0.0650	0.4193	
		polydot	NA	2	7.93	0.37			0.0517	0.4595	
		polydot	NA	1	1.72	5.20			0.0537	0.4411	
		polydot	NA	1	1.08	-5.24			0.0785	0.2932	
		ShB	polydot	NA	3	2.30	1.08			0.0413	0.2341
	polydot		NA	3	1.20	4.15			0.0413	0.2342	
	OMcT	polydot	NA	3	7.67	9.30			0.0551	0.2191	
Statistics	Avg.	polydot: 9	0.41	2.33	3.84	1.27			0.0571	0.3630	
	S.D.	laplacedot:3	0.05	0.82	2.76	4.17			0.0100	0.0883	
SVM		C	ϵ	Kernel	σ	Degree	Scale	Offset	RMSE	MXAE	
	TbPT	0.81	0.07	polydot	NA	7	2.73	5.87	0.0626	0.3777	
	TqA	2.81	0.41	polydot	NA	1	4.03	-2.09	0.0545	0.4953	
		2.81	0.51	polydot	NA	1	4.77	-3.81	0.0580	0.4925	
		3.53	0.28	polydot	NA	1	5.60	0.08	0.0541	0.5057	
		3.71	0.12	polydot	NA	1	5.67	0.69	0.0534	0.5062	
		3.14	0.72	rbfdot	0.05	NA	NA	NA	0.0754	0.4358	
	ShB	9.77	0.13	laplacedot	0.37	NA	NA	NA	0.0466	0.3238	
		7.56	0.85	polydot	NA	4	1.11	6.61	0.0600	0.2558	
		3.26	0.86	polydot	NA	4	2.57	5.81	0.0600	0.2748	
		9.32	0.43	polydot	NA	5	1.34	2.64	0.0586	0.2856	
		9.81	0.05	laplacedot	0.46	NA	NA	NA	0.0465	0.3295	
	OMcT	9.20	0.05	polydot	NA	2	9.25	2.96	0.0730	0.2576	
		7.34	0.69	polydot	NA	2	9.27	2.64	0.0808	0.2231	
	Statistics	Avg.	5.62	0.40	polydot: 10 laplacedot:2	0.29	2.8	4.63	2.14	0.0603	0.3664
		S.D.	3.12	0.30	rbfdot: 1	0.18	1.99	2.76	3.29	0.0101	0.1034
RFR		Trees	NF	Min TS	Max TN				RMSE	MXAE	

	TbPT	773	10	1	304		0.0463	0.4169	
	TqA	569	9	1	682		0.0953	0.4414	
		844	1	1	982		0.1152	0.4327	
		496	14	26	346		0.1122	0.4383	
		161	14	1	1,000		0.0955	0.4402	
		532	1	7	974		0.1176	0.4274	
		80	14	3	920		0.0957	0.4383	
		457	14	1	1,000		0.0947	0.4438	
	ShB	718	7	1	1,000		0.0454	0.2975	
		415	7	1	475		0.0457	0.2963	
	OMcT	879	9	1	493		0.0795	0.3768	
		153	9	1	590		0.0795	0.3752	
		463	9	1	564		0.0795	0.3756	
Statistics	Avg.	503.1	9.1	3.5	717.7		0.0848	0.4000	
	S.D.	249.9	4.3	6.7	259.5		0.0246	0.0506	
ANN		Hidden neurons	Activation	Optimizer	Batch size	Learning rate	Momentum	RMSE	MXAE
	TbPT	26	relu	sgd	199	0.77	0.83	0.0473	0.2945
		45	relu	sgd	199	0.77	0.73	0.0423	0.3186
	TqA	19	relu	adagrad	108	0.57	NA	0.0506	0.4503
		97	relu	adagrad	146	0.43	NA	0.0514	0.4183
		65	relu	adagrad	166	0.55	NA	0.0803	0.3799
		26	relu	adagrad	196	0.13	NA	0.0490	0.4699
	ShB	8	tanhdot	adagrad	85	0.30	NA	0.0405	0.2571
		7	tanhdot	adagrad	86	0.30	NA	0.0394	0.2682
		14	tanhdot	adagrad	184	0.38	NA	0.0395	0.2626
	OMcT	36	tanhdot	sgd	98	0.97	0.92	0.0421	0.1585
Statistics	Avg.	34.3	relu: 6	sgd: 3	146.7	0.52	0.83	0.0482	0.3278
	S.D.	26.9	tanhdot: 4	adagrad: 7	45.9	0.25	0.08	0.0115	0.0942

Supplemental Material Section B:

B.1 Hyperparameters effect on GPR

The only hyperparameters in GPR are kernel-related parameters, that is, the four kernel functions in Equation 16. The GPR performance with different $\text{Sigma}(\sigma)$ is plotted in Figure B.1 (a) and (b) for radial basis and Laplacian kernel, respectively. The low $\sigma(< 2)$ level takes a critical effect. The best GPR performance σ are 1 and 0 for radial basis and laplacian kernels, respectively.

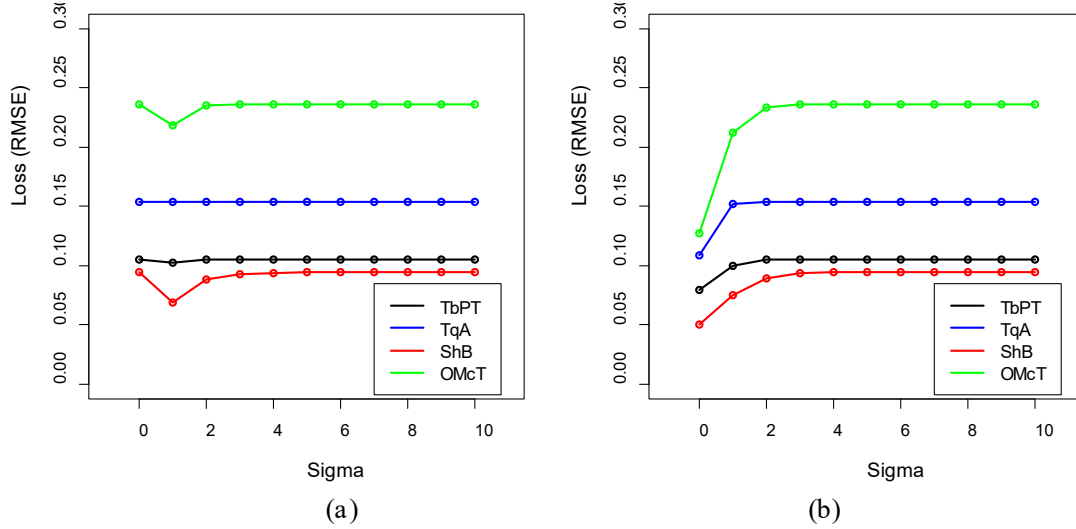


Figure B.1 Effects of kernel hyperparameter sigma on the GPR performance for (a) radial basis dot and (b) Laplacian kernels

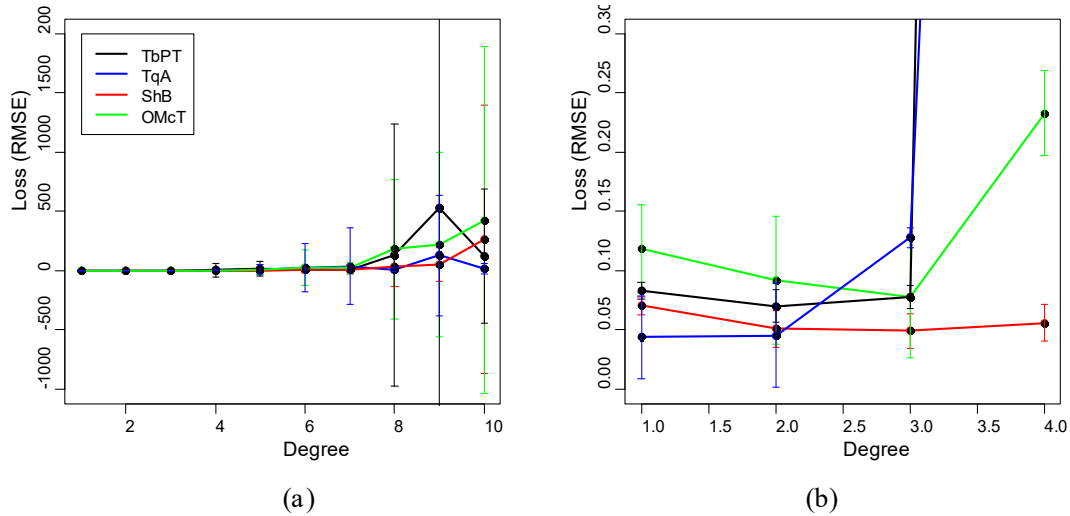


Figure B.2 The effect of polynomial degree on GPR performance with the error to account the influence of the scale and offset : (a) the whole range of degree and (b) the enlarged view on the low degree level

Regarding the polynomial kernel, different degrees influence model accuracy significantly. Table 4 shows that the optimal degrees would be 2 or 3, so low degree levels in Figure B.2(a) is amplified to see the details in Figure B.2(b). The 2nd or 3rd order polynomial also presented a high model accuracy. The influence of scale and offset was increased with the degree, which is indicated by the larger standard errors.

Furthermore, for *scale* and *offset*, their absolute values should be larger than 1 since this will significantly reduce the RMSE error as shown in Figure B.3. If their absolute values are larger than 1, it generally works well to generate an accurate GPR. The hyperbolic tangent kernel also contains the parameters of *scale* and *offset*. Figure B.4 shows their influence on GPR performance, which indicates a similar trend in four cases. The *scale* and *offset* are suggested to be around 1 and 10, respectively, for an accurate GPR.

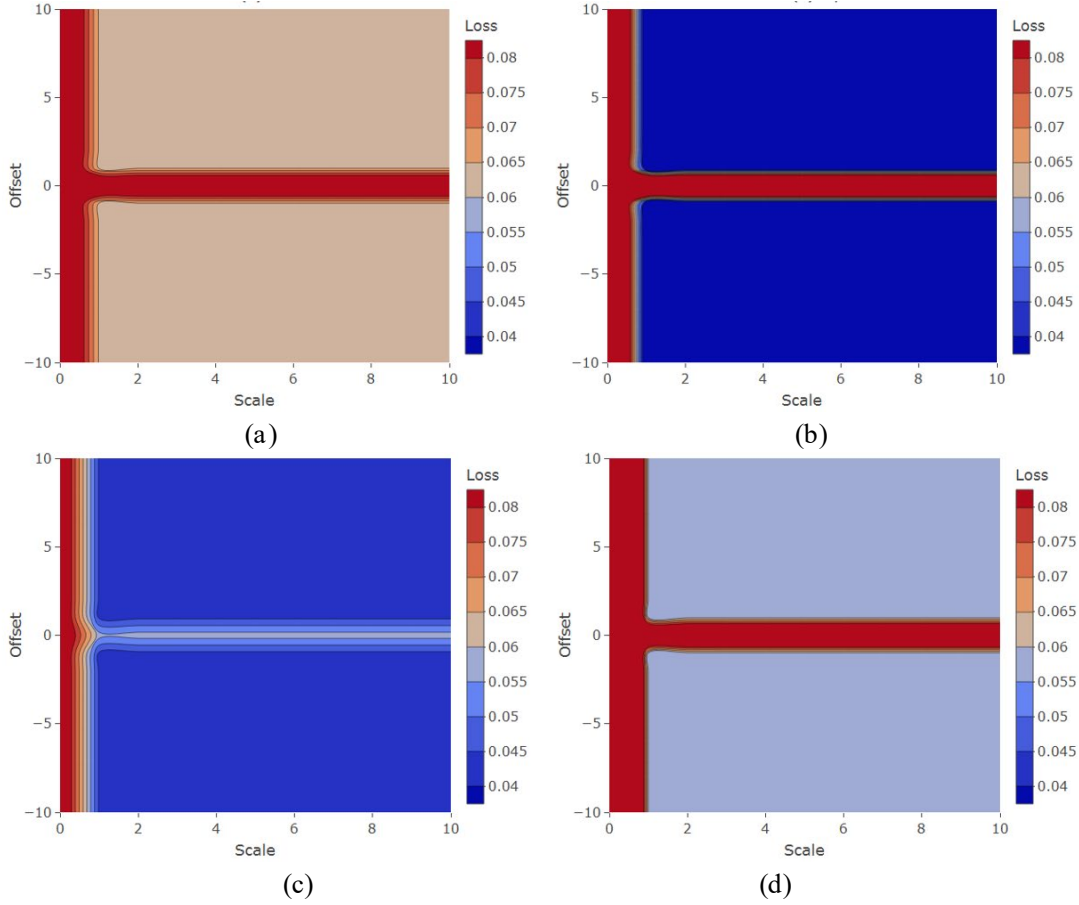
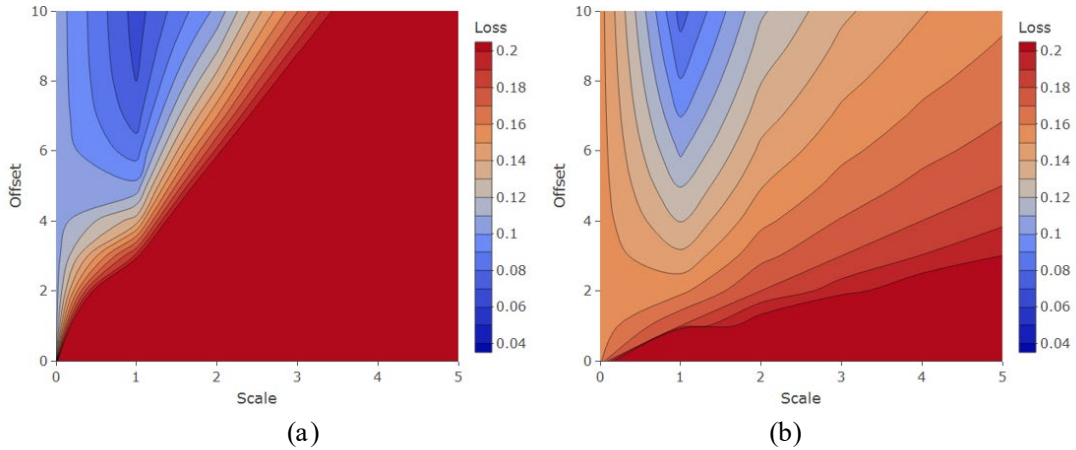


Figure B.3 GPR performance with different *scale* and *offset* under the *degrees* of (a) ShB with degree 3; (b) OMcT with degree 3; (c) TbPT with degree 2; (d) TqA with degree 2



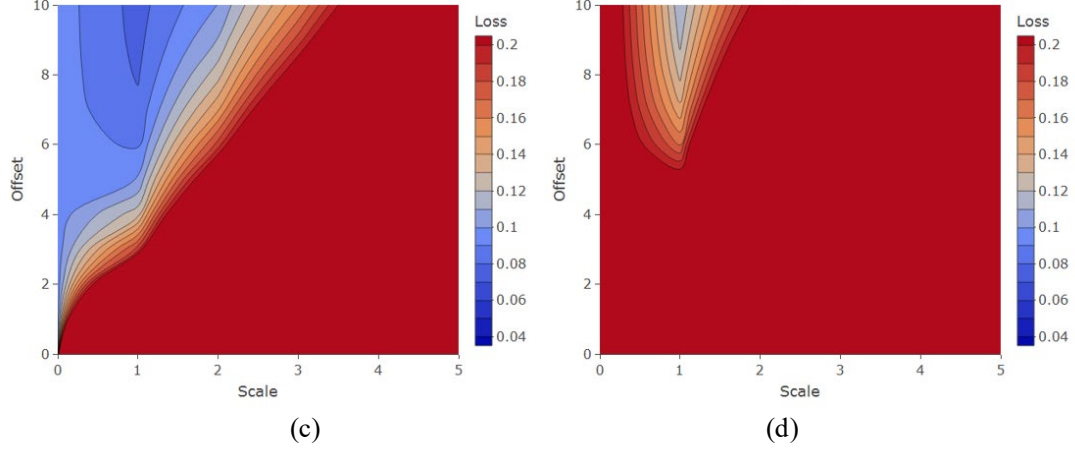


Figure B.4 GPR performance with the change of the hyperbolic tangent kernel function's *scale* and *offset* for (a) ShB; (b) OMcT; (c) TbPT; (d) TqA

In summary, the RMSE accuracy of sixteen models trained with the best kernel hyperparameters values is presented in Figure B.5. The polynomial kernel shows the best performance on GPR accuracy. Meanwhile, the radial basis kernel demonstrates a large scatter and less unstable performance.

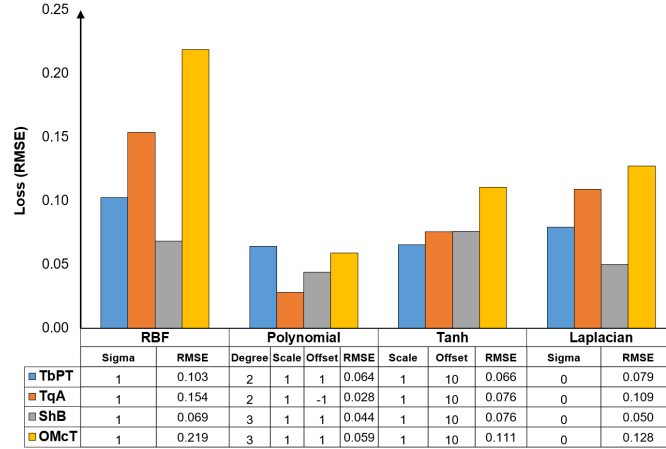


Figure B.5 Comparison on the modeling performances of the four kernel functions in the GPR algorithm

B.2 Hyperparameters effect on ANN

To explore the hyperparameters effect of ANN, a basic one-hidden-layer ANN is constructed with the following hyperparameter values based on the optimization: batch size=100, learning rate=0.1, hidden neurons=20, optimizer=sgd, activation function=tanh, momentum=0.9. Also, only the ShB dataset is used considering the high computational cost of ANN training and the similar trend of hyperparameters effect for each dataset. All models in this part are trained with 10,000 epochs.

The influence of batch size and the learning rate is studied and plotted with log scale contour in Figure B.6. Larger learning rates and smaller batch sizes speed up the convergence, but too large learning rates could lead to unstable training and may lose the optimum. However, too small mini-batch size could increase the communication cost, i.e. the computational cost to synchronize the shared variables (gradient or model parameters, etc.) between different mini-batches, although it could increase the convergence speed [1]. Base on Figure B.6, a learning rate of 0.1 is determined as the optimum. Under this condition, the larger

mini-batch size is preferred only if the same accuracy can be achieved to reduce communication costs [1]. Therefore, the mini-batch size is set as 100 for the current dataset size.

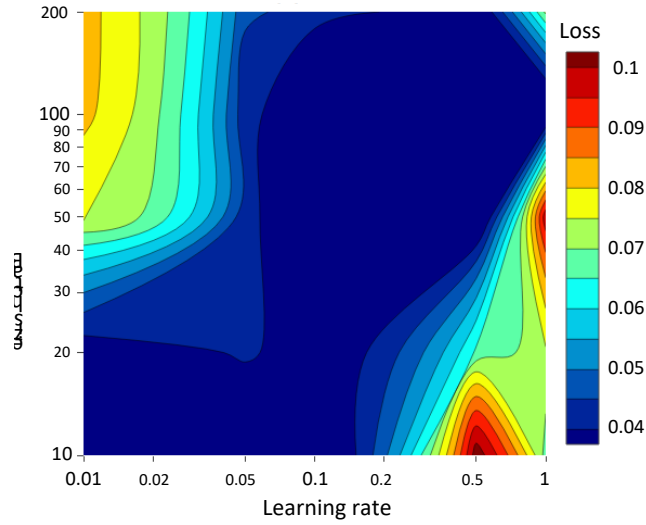


Figure B.6 Mutual influence of the learning rate and mini-batch size on ANN loss (RMSE) in log-scale

The influences of other hyperparameters, i.e. the hidden neuron, optimizer, activation function, and layer structures, on the convergence process are illustrated in Figure B.7. Figure B.7(a) shows that more hidden neurons, indicating more weight factors to be optimized, would slow down the training convergence. Considering the training dataset size (i.e. 1,000) in this part, 20 hidden neurons are used since it results in slightly better accuracy than the 5. In Figure B.7(b), among four optimizers, *adagrad* results in the highest accuracy, stability, and convergence speed. Although the *sgd* shows a similar accuracy, it is limited by the low convergence speed caused by its complicated training process [2]. Hence, *adagrad* would be a good choice.

In Figure B.7(c), *relu* shows low RMSE accuracy due to its linear behavior in Figure 2. After the transmission through one hidden layer with the linear activation function, the output of ANN will be still linear, which is not suitable for the problems with a non-linear response, such as ShB. Except for *relu*, the other three activation functions are all nonlinear and generated similar accuracy levels. The *tanh* reaches a quick and stable convergence due to its large value variation in the range of [0 1]. Therefore, *tanh* is used for the nonlinear response prediction.

As discussed, a multi-layered ANN possesses a higher ability to learn high nonlinear responses. To explore the multi-layers effect on ANN training, another four multi-layered models are built with optimal hyperparameters identified earlier. As shown in Figure B.7(d), 7-20-1 presents the best performance. The model 7-10-5-1 suggests a good but slightly lower accuracy since its number of weights (i.e. 125) is also less than a quarter of the training dataset size. The other three ANN structures greatly increase the number of weights and lead to unstable convergence process and deteriorated accuracy, which indicates insufficient training. This means compared with increasing the number of layers, the number of weights is more important to fully train an accurate ANN.

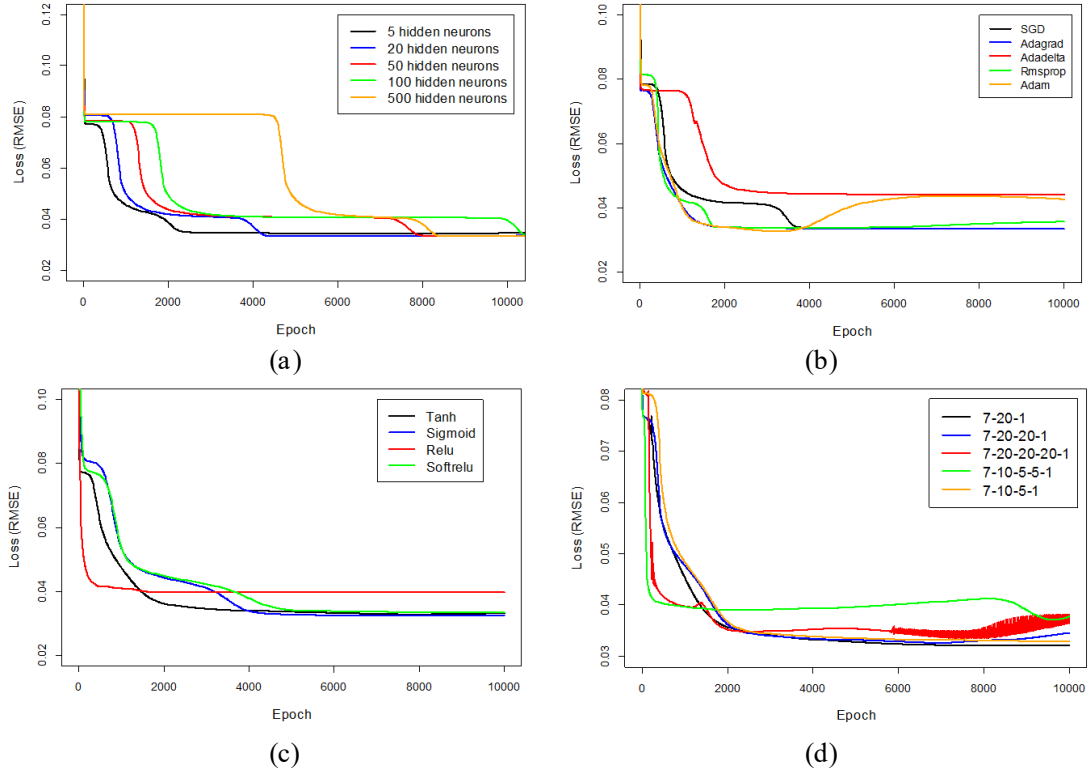


Figure B.7 Loss convergence histories in ANN models with respect to the (a) hidden neurons; (b) optimizers; (c) activation functions and (d) hidden layer structures, where 7-20-1 denotes 7 input features, 20 hidden layer neurons, and 1 output. The other ANN models are denoted in a similar manner.

Supplemental Material Section C:

Table C.1 The characteristics of the four design benchmark structures

Categories	Items		TbPT		TqA		ShB		OMcT	
MLA	Measure		Before after HOpt		Before after HOpt		Before after HOpt		Before after HOpt	
GPR	RMSE	Mean	0.085	0.069	0.048	0.048	0.046	0.041	0.073	0.059
		SD	0.013	0.009	0.018	0.020	0.008	0.002	0.006	0.004
	MXAE	Mean	0.539	0.401	0.421	0.451	0.349	0.247	0.335	0.255
		SD	0.163	0.143	0.333	0.342	0.101	0.030	0.069	0.045
	Time/s	Mean	0.532	0.428	0.528	0.416	0.530	0.446	0.506	0.592
SVM	RMSE	Mean	0.086	0.072	0.043	0.051	0.054	0.043	0.072	0.072
		SD	0.016	0.010	0.022	0.018	0.015	0.012	0.006	0.005
	MXAE	Mean	0.583	0.481	0.430	0.447	0.501	0.291	0.352	0.280
		SD	0.162	0.135	0.360	0.316	0.151	0.143	0.064	0.051
	Time/s	Mean	0.054	0.034	0.042	0.140	0.050	0.046	0.064	92.18
RFR	RMSE	Mean	0.057	0.049	0.097	0.092	0.054	0.046	0.086	0.081
		SD	0.014	0.006	0.009	0.010	0.011	0.007	0.010	0.006
	MXAE	Mean	0.413	0.374	0.425	0.404	0.421	0.284	0.398	0.358
		SD	0.165	0.082	0.214	0.185	0.144	0.087	0.072	0.070
	Time/s	Mean	1.102	4.406	1.158	3.738	0.786	3.920	0.904	5.350
ANN	RMSE	Mean	0.093	0.051	0.050	0.051	0.072	0.039	0.077	0.043
		SD	0.015	0.008	0.021	0.013	0.011	0.005	0.003	0.003
	MXAE	Mean	0.619	0.346	0.482	0.452	0.564	0.262	0.309	0.177
		SD	0.144	0.091	0.373	0.207	0.212	0.090	0.034	0.024
	Time/s	Mean	21.56	19.51	21.76	33.81	21.44	42.55	20.92	32.05

References:

- [1] Li, M., et al. Efficient mini-batch training for stochastic optimization. in Proceedings of the 20th ACM SIGKDD international conference on Knowledge discovery and data mining. 2014. ACM.
- [2] Lee, S., et al., Background Information of Deep Learning for Structural Engineering. Archives of Computational Methods in Engineering, 2017. 25(1): p. 121-129.